Schweizerische Eidgenossenschaft
Confédération suisse
Confederazione Svizzera
Confederaziun svizra

Départmenet fédéral de l'environnement, des transports,
de l'énergie et de la communication DETEC

Ofiice fédéral de l'énergie OFEN

Rapport final 12 octobre 2011

Dimensionnement des galeries et puits blindés

Design of steel lined pressure tunnels and shafts

Mandant:
Office fédéral de l'énergie OFEN
Programme de recherche Force hydraulique
CH-3003 Berne
www.bfe.admin.ch

Cofinancement:
Competence Center for Energy and Mobility CCEM-CH, CH-5232 Villigen PSI

Mandataire:
Ecole Polytechnique Fédérale de Lausanne EPFL
Laboratoire de Constructions Hydrauliques LCH
Station 18
CH-1015 Lausanne
lchwww.epfl.ch

Auteurs:
Fadi Hachem, EPFL-LCH, fadi.hachem@epfl.ch
Prof. Dr. Anton Schleiss, EPFL-LCH, anton.schleiss@epfl.ch

Responsable de domaine de l'OFEN: Dr. Michael Moser
Chef de programme de l'OFEN: Dr. Klaus Jorde
Numéro du contrat de l'OFEN: SI/500169-01

Table des matières

Vorwort

Dieser Schlussbereicht fasst die für die Praxis wesentlichen Ergebnissen des Forschungsprojektes in einer französischen Artikel zusammen, welcher 2012 in der Fachzeitschrift „wasser, energie, luft“ publiziert wird.

Im Anhang sind wissenschaftliche Publikationen angefügt welche im Jahre 2011 zur Publikation akzeptiert wurden oder bereits veröffentlicht sind.

Die detaillierten Resultate des Forschungsprojektes wurde als Dissertation No. 5171 unter dem Titel „Monitoring of Steel-Lined Pressure Shafts Considering Water-Hammer Wave Signals and Fluid-Structure Interaction“ veröffentlicht. Sie wird auch als Communication 48 du Laboratoire de constructions hydrauliques (LCH) erscheinen.

Dimensionnement et surveillance des puits blindés en considérant les coups de bélier et l'interaction fluide-structure

■ *Fadi E. Hachem, Anton J. Schleiss*

Résumé

En raison de la forte demande de l'énergie de pointe, les centrales hydro-électriques opèrent actuellement d'une manière brutale pour assurer avec efficacité, flexibilité et sécurité l'équilibre entre la production et la demande. Les marges de sécurité liées aux sollicitations dynamiques générées par l'eau dans les puits et tunnels blindés se trouvent de plus en plus réduites surtout avec l'utilisation des aciers de blindage à haute résistance dans les nouvelles centrales hydro-électriques. Dans ce contexte, une nouvelle base de dimensionnement et une approche novatrice de surveillance sont présentées avec une attention particulière sur le phénomène d'interaction fluide-structure entre l'eau et la paroi de ces structures. Le modèle théorique proposé peut être considéré comme base pour le développement des nouveaux critères de dimensionnement qui considèrent la mécanique de rupture fragile dans l'analyser de la réponse du blindage. D'autre part, l'influence de la détérioration locale de la rigidité de la paroi des puits et tunnels blindés sur la célérité et l'atténuation de l'onde de coup de bélier est étudiée expérimentalement. Une méthode de surveillance pour détecter la formation, l'endroit et la sévérité de ces faiblesses est présentée. Une série de mesures sur le puits blindé d'un aménagement de pompage-turbinage en Suisse a été également effectuée pour valider le concept de surveillance proposé.

1. Introduction

Les offres du marché de l'électricité de pointe et de réglage énergétique offrent une excellente opportunité aux centrales hydro-électriques de pompage-turbinage d'augmenter leur production tout en gardant des marges de sécurité acceptables. En plus de son prix attractif, cette énergie est essentielle pour éviter le black-out qui pourrait couvrir des grandes régions et causer des pertes économiques importantes.

Un consortium technique nommé HydroNet I (http://hydronet.epfl.ch) a été créé en 2007 dans le but de définir des nouvelles méthodologies de dimensionnement, de fabrication, d'opération, d'auscultation et de contrôle de ces centrales. L'objectif stratégique de ce consortium est de maintenir la position privilégiée de la Suisse dans le domaine de la production hydro-électrique et dans l'exportation de la haute technologie.

Le Laboratoire de Constructions Hydrauliques (LCH) de l'Ecole Polytechnique Fédérale de Lausanne (EPFL) a été désigné responsable de la branche génie civil de HydroNet I. Deux thèses ont été définies avec comme sujets: (i) comprendre l'influence de pompage-turbinage sur la sédimentation des réservoirs et (ii) le dimensionnement et l'auscultation des puits et tunnels blindés. C'est ce dernier qui fait l'objet de cet article où les objectifs suivants sont visés:

1. Amélioration des bases de dimensionnement par une étude théorique qui pourra être le point de départ pour des futurs développements incluant les méthodes de la mécanique de rupture fragile pour analyser la réponse et la sécurité des blindages fabriqués en acier à haute résistance.
2. Développement de nouvelles méthodes et approches d'auscultation non-intrusives basées sur l'analyse des signaux transitoires générés par les coups de bélier et sur le phénomène d'interaction fluide-structure. Ces méthodes sont capables de détecter la formation, l'emplacement et la sévérité d'une importante détérioration de la rigidité de la paroi des puits et tunnels blindés par le moyen de traitement et d'analyse des pressions dynamiques mesurées à leurs deux extrémités accessibles.

2. Modèle mathématique de dimensionnement

La recherche bibliographique (Hachem & Schleiss, 2009) a montré que les méthodes de dimensionnement quasi-statiques utilisées actuellement sont basées sur l'idée de maintenir la contrainte de traction dans l'acier du blindage au-dessous de la limite d'élasticité de l'acier utilisé. D'autres critères liés à des détails de construction et à des limites de tolérance sont également respectés pour diminuer le risque de formation des contraintes locales excessives dans le blindage. Ces méthodes de dimensionnement ainsi que l'analyse de la sécurité des puits et tunnels blindés sont devenues insuffisantes pour dimensionner les blindages fabriqués à partir des aciers à haute résistance dans les nouvelles centrales hydro-électriques. Les problèmes engendrés par l'utilisation de ce type d'acier, notamment la rupture fragile et la fatigue, obligent les chercheurs à améliorer et/ou modifier le modèle théorique actuel de calcul.

Dans une première étape, des approches générales pour estimer la vitesse de propagation des coups de bélier à l'intérieur des puits et tunnels blindés ont été analysées dans le cas quasi-statique, c'est-à-dire, sans considérer l'interaction fluide-structure (FSI) et la dépendance entre la vitesse et la fréquence (Hachem & Schleiss, 2011a). Les conditions aux bords ainsi que les hypothèses prises en considération dans l'établissement de ces approches ont été présentées et discutées en détail. Les expressions reformulées de la célérité ont été également comparées à d'autres formules qui sont actuellement utilisées. Dans le cas des blindages en acier de faible épaisseur entourés de rocher à faible module d'élasticité, les relations proposées par Jaeger (1977) et Parmakian (1963) surestiment la vitesse des ondes de l'ordre de 3 à 4.5% alors que dans la formule de Halliwell (1963), la surestimation atteint 7.5%. La vitesse quasi-statique des ondes est significativement influencée par l'état du béton de remplissage et du rocher entourant le blindage (fissuré ou pas). Dans le cas où ces deux matériaux sont considérés comme fissurés, la vitesse quasi-statique est surestimée entre 1% et 8% relativement au cas du béton et rocher non fissurés. En fonction du degré de rigidité de blindage, le FSI engendre des différences significatives dans la vitesse des coups de bélier.

Dans une deuxième étape, un modèle basé sur le phénomène d'interaction fluide-structure (FSI) a été proposé (Hachem & Schleiss, 2011a) pour le développement des nouveaux critères de dimensionnement qui considèrent la mécanique de rupture fragile pour analyser la réponse du blindage en acier à haute résistance. Dans ce modèle *(figure 1)*, le béton de remplissage et la roche fissurée entourant le blindage sont modélisés dans les deux directions longitudinales et transversales par un système constitué d'un ressort de rigidité, K_{sr}, d'un amortisseur, C_r, et d'une masse additionnelle, M_r. L'équation de dispersion quadratique résultante de ce modèle FSI a montré la dépendance entre la rigidité de la paroi des puits (caractérisée par les coefficients K_{sr}, C_r et M_r) et deux paramètres importants, à savoir, la vitesse de propagation et l'atténuation de l'amplitude des ondes de pression. Ces deux paramètres peuvent donc être considérés comme indicateurs globaux pour détecter le changement de rigidité des parois de ces structures. La résolution de l'équation de dispersion dans le domaine fréquentiel par le biais d'un exemple numérique, a montré que dans l'intervalle des hautes fréquences (supérieure à 600 Hz), l'approche FSI génère des vitesses d'onde 13% au-dessus de celles obtenues dans le cas quasi-statique. Cette différence de vitesse peut atteindre les 150% pour les fréquences entre 150 Hz et 300 Hz. Dans l'intervalle [80 Hz ; 800 Hz], le mode de propagation lié aux ondes précurseurs présente une basse fréquence de coupure qui dépend de la distribution longitudinale de la rigidité du blindage. Le premier mode d'onde acoustique commence à propager à partir d'une fréquence proche de 525 Hz. La fréquence de coupure relative à ce mode est fonction de la rigidité radiale du blindage. Dans la pratique, la différence de vitesse des coups de bélier entre le cas FSI et le cas quasi-statique est considérée comme tolérable en raison de l'incertitude dans l'estimation des propriétés mécaniques du rocher et de la présence de l'air dans l'eau. Les pressions dynamiques obtenues par l'approche théorique classique des coups de bélier sont peut influencées par cette différence de vitesse de l'onde alors que le FSI peut engendrer des pressions dynamiques extrêmes à hautes fréquences.

La validation du modèle théorique proposé sera faite dans une seconde thèse qui se déroulera dans le cadre du projet HydroNet II. Cette validation par modélisation numérique et mesures sur modèle physique et sur prototype permettra le développement des nouvelles méthodes et procédures de dimensionnement pour les puits blindés. Les résultats de ces analyses fourniront des précieuses informations aux producteurs hydro-électriques en Suisse surtout suite à la rupture du puits blindé de l'aménagement Cleuson-Dixence générée par le développement et propagation des microfissures dans les soudures de l'acier du blindage à haute résistance.

3. Surveillance non-intrusive des puits et tunnels blindés

3.1 Description du phénomène physique

En parallèle au développement d'une procédure moderne de dimensionnement pour les nouvelles constructions, l'auscultation des ouvrages existants s'avèrent primordiale pour la maitrise du risque résiduel lié à leur rupture sous l'effet de la pression interne dynamique de l'eau acheminée. Une nouvelle méthode de surveillance non-intrusive a été proposée pour détecter à temps réel et sous certaines conditions, la formation, l'endroit et la sévérité d'une éventuelle faiblesse locale de la rigidité de la paroi des puits blindés.

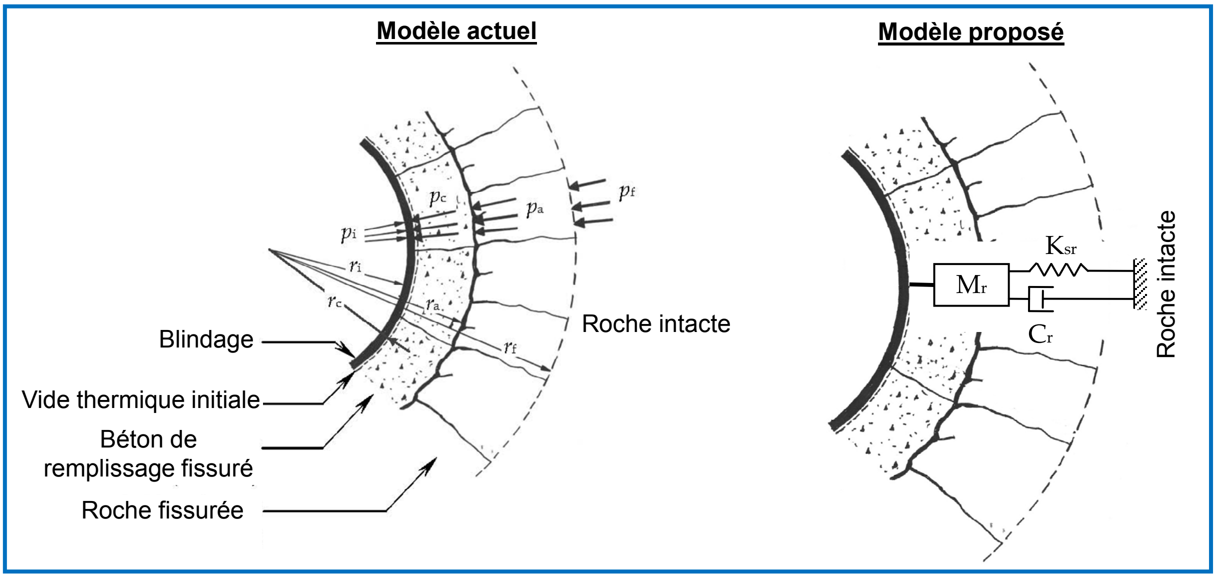

Figure 1. Modèle théorique actuel et celui proposé pour le dimensionnement des puits et tunnels blindés.

En effet, la détérioration locale de la rigidité de la paroi de ces structures crée un changement des paramètres hydroacoustiques de la région concernée (changement de la célérité de l'onde, *a* et/ou de la section de l'écoulement, *A*) (Wylie & Suo, 1993, Hachem & Schleiss, 2010). Les limites (ou jonctions) de ces régions affaiblies constituent des barrières sur lesquelles une onde incidente sera décomposée en une onde qui transite vers l'aval et une autre qui se réfléchit vers l'amont *(figure 2)*. L'idée clef de la méthode de surveillance repose sur l'analyse et le traitement de ces signaux de pression dynamique et de la vibration radiale du blindage engendrée par celle-ci et mesurés aux deux extrémités accessible du puits.

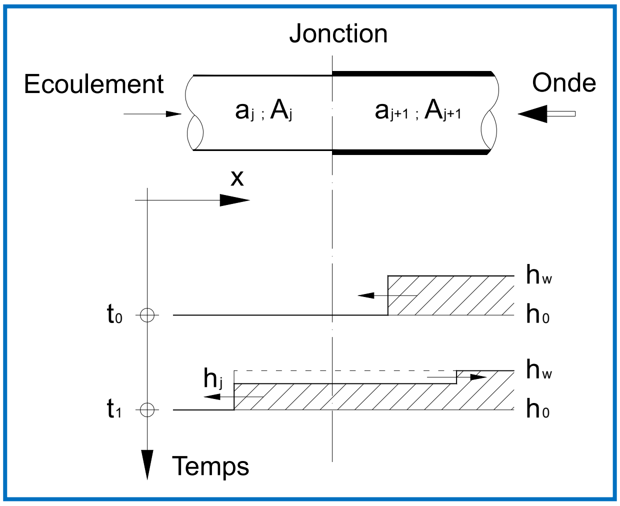

Figure 2. Transition et réflexion d'une onde de pression incidente (h_w-h_0) en traversant une jonction qui sépare deux régions de puits de caractéristiques hydroacoustiques distinctes.

3.2 Vérification par des essais sur modèle physique à échelle réduite

3.2.1 Description de l’installation d’essai

L'influence de la détérioration locale de la rigidité de la paroi des puits et tunnels blindés sur la célérité et l’atténuation de l'onde de pression durant les phénomènes transitoires a été étudiée expérimentalement. La formation des régions de puits de faible rigidité est une conséquence de la détérioration de la résistance du béton de remplissage et du massif rocheux qui entourent le blindage. Une méthode innovatrice pour détecter la présence de ces portions de faible rigidité a été proposée et validée par des séries d'essais sur modèle physique à échelle réduite (Hachem & Schleiss, 2011b).

L’installation est constituée d’une conduite d’essai de 150 mm de diamètre intérieure et de 6.25 m de longueur *(figure 3)*. Un réservoir, une pompe à vitesse variable et une conduite en PVC alimentent en eau un réservoir à air comprimé situé à l’amont de la conduite d’essai. Cette dernière est construite par l’assemblage de plusieurs pièces de longueurs égales à 0.5 m et 1 m. Les flasques de connexion servent comme points de fixation de la conduite d’essai contre la dalle et le mur en béton du laboratoire. Une vanne type guillotine équipée par un piston à air comprimé assure la fermeture rapide et la génération des coups de bélier dans la conduite d’essai. Un compresseur alimente le piston de la vanne par le volume et la pression d’air nécessaire pour son fonctionnement. Deux capteurs infrarouges indiquent les positions de fermeture et d’ouverture complète de la vanne guillotine. Un débitmètre, deux vannes de sécurité et deux raccordements flexibles complètent le circuit fermé du stand d’essai. L’acquisition des données a été faite en utilisant deux capteurs de pression type ”HKM-375M-7-BAR-A, Kulite”, deux géophones type ”I/O Nederland, SM-6 4.5Hz 3500 ohm”, une carte d’acquisition ”NI-USB-6259-M” et un ordinateur équipé par un programme de contrôle et d’acquisition préparé sur le plateforme du logiciel LabVIEW 8.6.

Un nombre total de 12 configurations différentes de la conduite d’essai ont été testées *(figure 4)*. Les bouts de faible rigidité ont été modélisés en remplaçant les parties en acier par d'autres fabriquées en aluminium ou PVC. Les mêmes conditions initiales stationnaires de débit et de pression ont été adoptées pendant les 12 essais répétitifs réalisés sur chacune des configurations présentées à la *figure 4*. Une description plus détaillée de l’installation physique est disponible dans Hachem (2011c).

3.2.2 Analyses des résultats expérimentaux

Les signaux des pressions dynamiques et des vibrations radiales de la paroi de la conduite d'essai ont été mesurés à ses deux extrémités (S1 et S2 sur la *figure 4*) durant les évènements des coups de bélier. Les signaux mesurés ont été traités et analysés dans Hachem & Schleiss (2011d and 2011e) en utilisant, entre autres, la transformation de Fourier (Lyons, 1997), les ondelettes (Mallat, 1990, Mathworks, 2008), la technique de cross-corrélation et la réponse fréquentielle du système (Lang, 1987, Shin & Hammond, 2008).

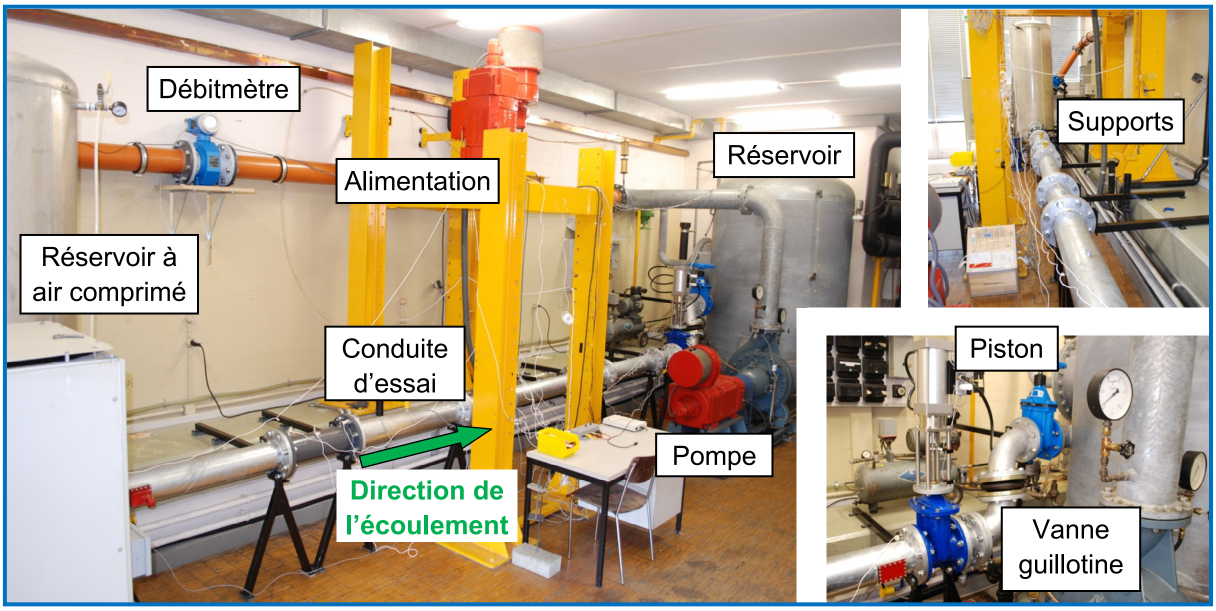

Figure 3. Modèle physique à échelle réduite construit au Laboratoire de Machines Hydrauliques (LMH) de l'Ecole Polytechnique Fédérale de Lausanne (EPFL).

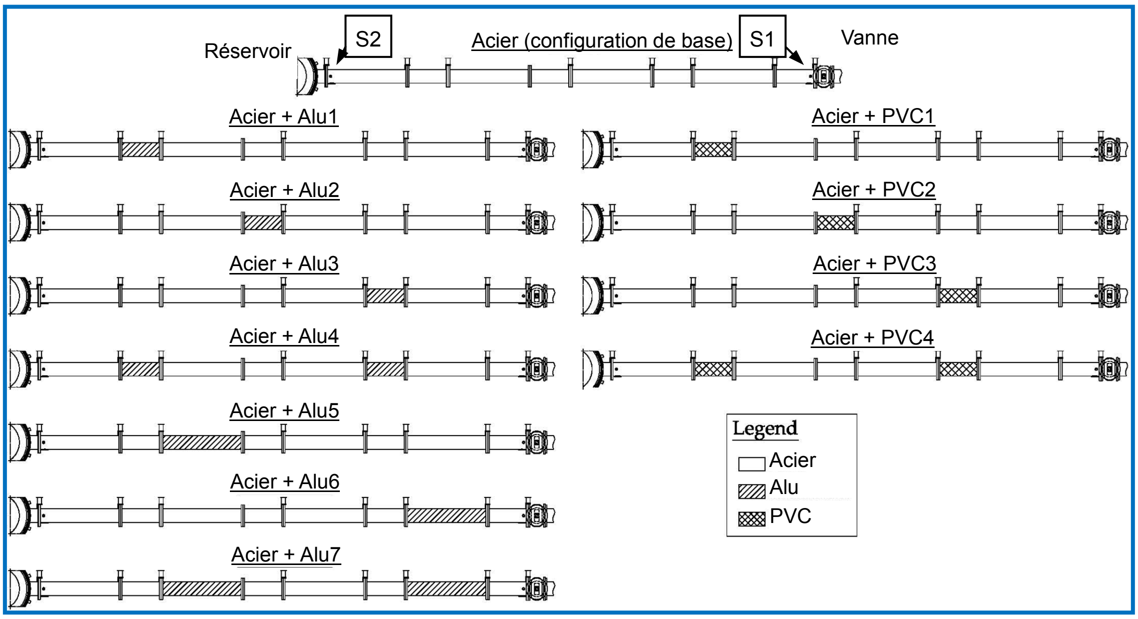

Figure 4. Les différentes configurations testées de la conduite d'essai de l'installation physique.

La *figure 5* présente les célérités et les atténuations de l'amplitude de l'onde de coup de bélier estimées à partir de l'analyse des pressions mesurées pendant les essais effectués sur les 12 configurations de la conduite. Le traitement des signaux des deux géophones par les fonctions de transfert a donné des résultats similaires à ceux obtenus à partir des mesures de pression avec une erreur relative maximale de l'ordre de 6%. Les résultats montrent que la célérité et l'atténuation de l'onde de pression sont deux facteurs qui peuvent être considérés comme indicateurs globaux de la formation d'une faiblesse locale importante dans la rigidité de la paroi des conduites, puits et tunnels blindés (Hachem & Schleiss, 2011f and 2011g).

L'association entre la technique de transformation de Fourier et les ondelettes a permis l'estimation des positions des limites de la pièce de conduite en PVC dans les configurations ''Acier+PVC1, 2 et 3''. Cela était possible dans le cas où des ondes à front raide ont été générées par la transmission de l'impact de l'air comprimé depuis le piston vers l'eau dans la conduite à travers l'axe verticale de la vanne guillotine. Les distances réelles et estimées ainsi que les erreurs relatives commises par cette estimation sont présentées à la *figure 6*. Une fois les deux limites de la faiblesse sont localisées, la sévérité du changement de la rigidité de la conduite a pu être estimée avec une erreur moyenne maximale de 20.6%.

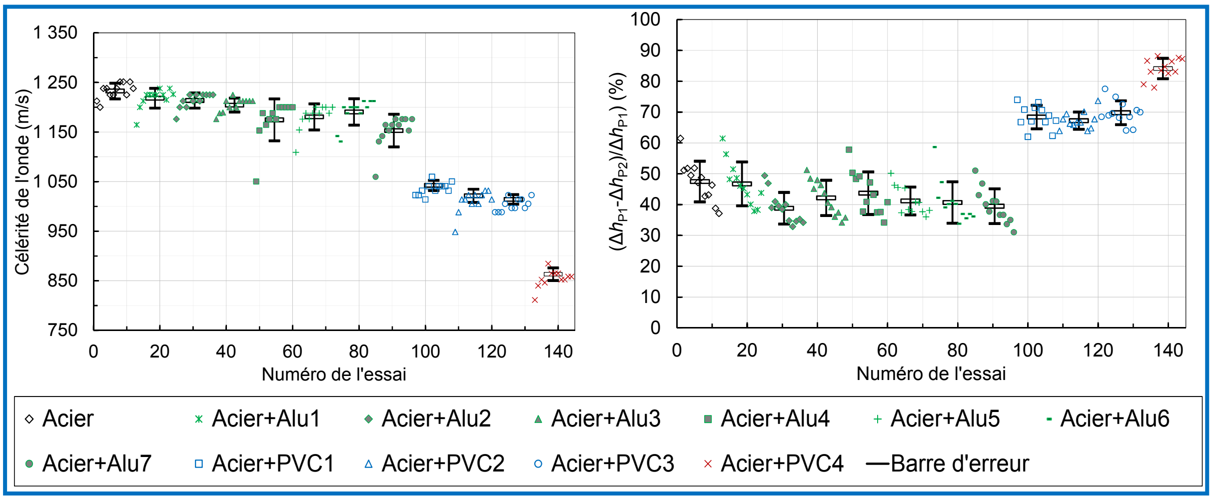

Figure 5. A gauche, les célérités de coup de bélier et, à droite, les atténuations de leur amplitude à l'intérieur de la conduite d'essai entre les points de mesures S1 et S2 pour les 12 configurations testées.

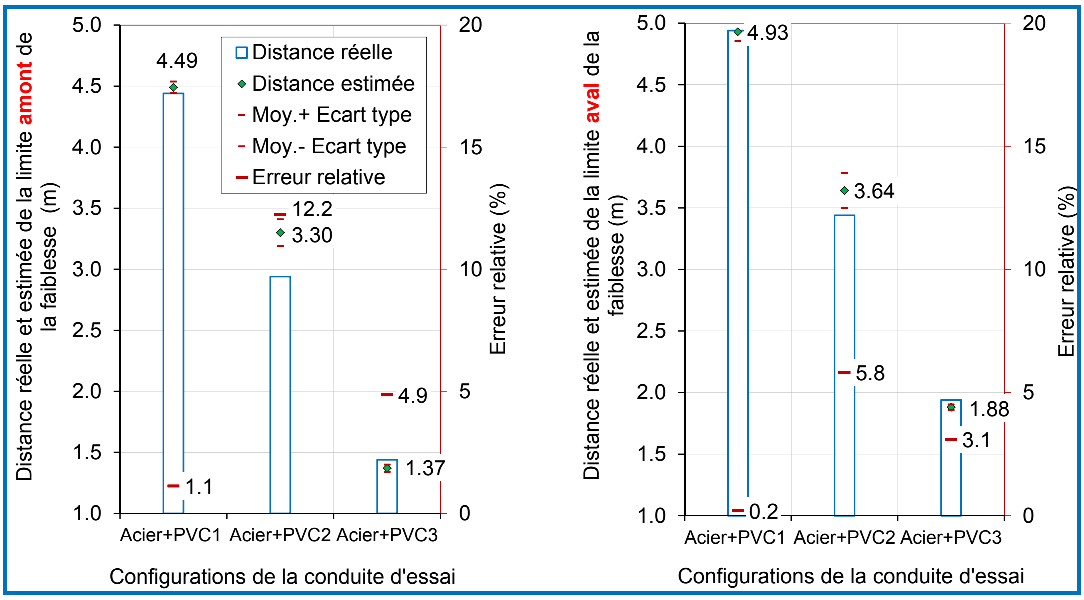

Figure 6. Moyennes et écart types des distances estimées de la limite amont (à gauche) et aval (à droite) de la faiblesse en PVC par rapport à la position de la station de mesure S1 pour les 3 configurations ''Acier+PVC1, 2 et 3''. Les distances réelles et les erreurs relatives sont encore présentées pour comparaison.

3.3 Application de la méthode de surveillance à l'échelle de prototype

3.3.1 Description du site

Le puits blindé de la centrale de pompage-turbinage de Grimsel II située dans le Canton de Bern en Suisse et propriété de la compagnie KWO (Kraftwerke Oberhasli AG), a été équipé par deux capteurs de pression et deux géophones. Ces capteurs ont été placés aux deux extrémités accessibles du puits blindé à l'entrée de la centrale et sur la vanne papillon de sécurité entre le système de chambre d'équilibre amont constitué par une chambre verticale et un puits incliné *(figure 7)*. Une description plus détaillée du site est disponible sur le site de KWO (www.grimselstrom.ch) et dans le rapport de thèse Hachem (2011c).

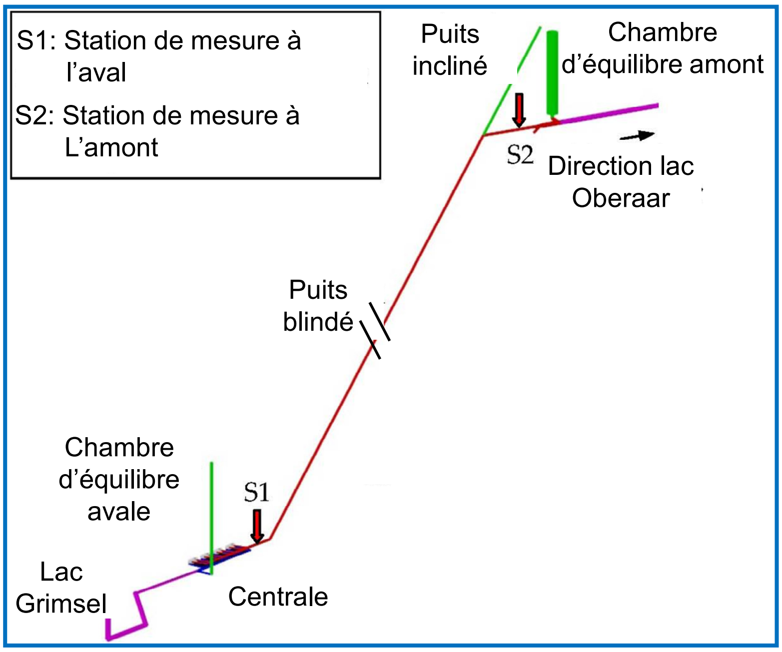

Figure 7. Schéma 3d du puits blindé de l'aménagement de pompage-turbinage de Grimsel II. Les deux stations de mesures S1 (à l'entrée de la centrale) et S2 (entre le puits incliné et la chambre d'équilibre verticale) sont encore indiquées.

3.3.2 Résultats et analyses des mesures effectuées sur le prototype

Des mesures in-situ ont été effectuées pour valider la méthode de détection et de localisation des bouts de puits de faible rigidité. Les données de pression et de vibration ont été récoltées d'une manière automatique et continue avec deux systèmes d'acquisition séparés. Ces systèmes ont été synchronisés par le moyen d'une connexion Ethernet via une fibre optique. Le contrôle et la récupération des données ont été effectués en ligne par le moyen d'une liaison internet sécurisée (VPN). Un nombre total de 396 fichiers de mesure ont été récoltés entre début février et début juin 2011. La *figure 8* montre un exemple des pressions dynamiques acquises par les deux capteurs de pression aux stations S1 et S2.

Il est à signaler que les petites amplitudes des variations de pression, le niveau relativement important du bruit et la sensibilité des géophones à ces bruits ont rendu difficile l'exploitation des mesures faites par ces capteurs.

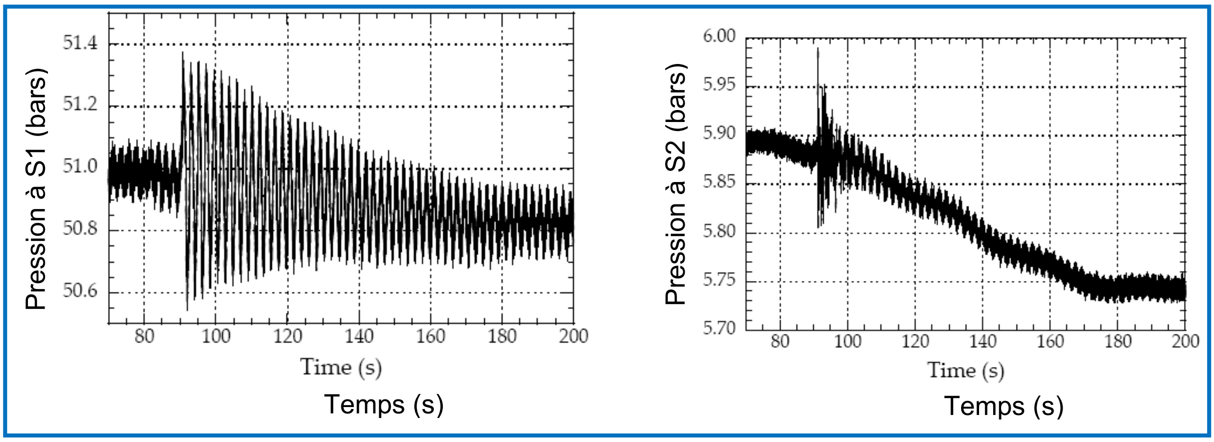

Figure 8. Pressions dynamiques mesurées aux deux stations S1 et S2 sur le puits blindé de Grimsel II durant l'arrêt d'une turbine.

Différentes approches ont été appliquées dans le but d'estimer la célérité et l'atténuation d'énergie de l'onde de pression générée par les coups de bélier durant l'enclenchement et l'arrêt des pompes et des turbines. Les faibles variations de pression dynamique de service combinées avec l'existence d'une masse rocheuse homogène entourant le blindage ont rendu difficile l'application de la totalité de la procédure de surveillance proposée. Néanmoins, des graphes de surveillance basés sur la méthode de contrôle de qualité (Montgomery, 2005) ont pu être établis pour les deux indicateurs, à savoir, la célérité et le coefficient exponentiel de dissipation de l'onde *(figure 9)* (Hachem & Schleiss, 2011h). La vitesse de l'onde a été estimée à partir de la transformation de Fourier des pressions mesurées à la station S1. Quant au coefficient d'atténuation, il a été déterminé par un calcul de RMS du signal de pression S1 suivi d'une régression exponentielle. Trois limites de contrôle qui représentent l'état actuel de la rigidité de la paroi du puits blindé ont été définies sur les graphiques de surveillance. Ces limites ainsi que les tendances globales des nuages des points actuels et futures seront utilisés pour surveiller la paroi du puits blindés. Les limites de contrôle relatives à la vitesse de l'onde doivent être révisées après l'acquisition d'une plus longue série de mesures. Les limites qui correspondent au coefficient exponentiel de dissipation de l'onde durant l'enclenchement des pompes et turbines peuvent être utilisées pour la surveillance du puits blindé. Durant les modes de fermeture des machines hydrauliques, les valeurs de coefficient de dissipation ont subi un changement de 55%. Pour expliquer ce décalage, des longues séries de mesure de pression sont nécessaires.

4. Conclusions

La demande importante de l'énergie de pointe provenant des centrales hydroélectriques exige des réglages rapides et multiples de la puissance des turbines et/ou des pompes. Les sollicitations dynamiques sont ainsi amplifiées et les marges de sécurité sont réduites. La rupture de blindage des puits et tunnels de ces centrales sous l'effet des pressions intérieures a des conséquences catastrophiques. Les pertes économiques et sociales générées par l'arrêt de production pour vider, ausculter et éventuellement réparer ces ouvrages sont considérables.

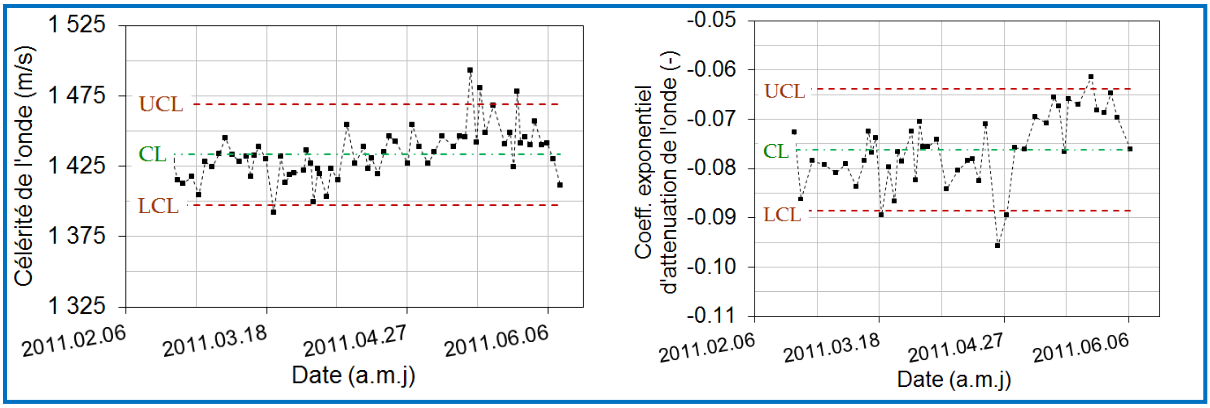

Figure 9. Graphiques de surveillance de la célérité (à gauche) et du coefficient exponentiel d'atténuation de l'onde (à droite) du puits blindé de la centrale de pompage-turbinage de Grimsel II.

La présente recherche fait partie du projet multidisciplinaire HydroNet I est vise à améliorer les méthodes de dimensionnement et à proposer des approches de surveillance non-intrusives des puits et tunnels blindés. Un modèle basé sur le phénomène d'interaction fluide-structure (FSI) a été proposé pour le développement des nouveaux critères de dimensionnement qui considèrent la mécanique de rupture fragile pour analyser la réponse du blindage en acier à haute résistance. Les pressions dynamiques obtenues par l'approche théorique classique des coups de bélier sont peut influencées par la différence de vitesse de l'onde quasi-statique. Néanmoins, le FSI peut engendrer des pressions dynamiques extrêmes et de haute fréquence. La validation du modèle théorique proposé par modélisation numérique et éventuellement par des mesures sur modèle physique et sur prototype sera faite dans le cadre d'une future thèse qui se déroulera sous le projet HydroNet II.

La nouvelle méthode de surveillance est validé expérimentalement et montre que la vitesse de propagation et le coefficient d'atténuation des ondes sont des bons indicateurs de la présence d'une faiblesse locale importante dans la rigidité radiale des puits et tunnels blindés. Cette méthode repose sur le traitement et l'analyse des signaux de pression et de vibration mesurés aux deux extrémités accessibles de ces ouvrages. Elle est capable de localiser l'endroit d'une seule et importante faiblesse. Quand des ondes à front raide sont générées, il est possible de localiser les deux extrémités de la faiblesse avec une erreur moyenne maximale de 5.9%. La sévérité du changement de la rigidité de la paroi a pu être estimée avec une erreur moyenne maximale de 20.6%.

Des mesures in-situ sur un aménagement de pompage-turbinage ont été effectuées pour valider la méthode de détection et de localisation des bouts de puits de faible rigidité. Les faibles variations de pression dynamique et l'existence d'une masse rocheuse homogène autour du blindage ont rendu difficile l'application de la totalité de la procédure de surveillance. Néanmoins, des graphes de surveillance pour la célérité et le coefficient exponentiel de dissipation de l'onde ont pu être établis. Trois limites de contrôle qui représentent l'état actuel de la rigidité de la paroi du puits blindé ont été définies sur ces graphiques. Ces limites ainsi que les tendances globales des nuages de points actuels et futures seront utilisés pour surveiller la paroi du puits blindé.

Remerciements

La présente recherche fait partie du projet interdisciplinaire HydroNet I qui est financé par *Swiss Competence Center Energy and Mobility* (CCEM-CH), *Swisselectric research* et l'*Office Fédéral de l'énergie* (OFEN). Les auteurs tiennent à remercier la *Fondation Lombardi* pour la précieuse aide financière dédiée à la construction du modèle physique expérimental. Un grand merci est également attribué à *Kraftwerke Oberhasli AG* (KWO) pour leur support technique offert durant les mesures sur le prototype. Une appréciation particulière est adressée à Madame Didia Covas pour ses commentaires et propositions formulés durant sa présence à l'EPFL comme professeur invité.

Références

Hachem, *F*., *Schleiss*, *A*. (2009). The design of steel-lined pressure tunnels and shafts. International Journal on Hydropower & Dams*,* 16(3),142-151.

Hachem, *F*., *Schleiss*, *A*. (2010). Influence of local stiffness of conduits on water hammer propagation signal. Proceedings of the First European IAHR Congress, www.iahr.net, Edinburgh.

Hachem, *F*., *Schleiss*, *A*. (2011a). A review of wave celerity in frictionless and axisymmetrical steel-lined pressure tunnels. Journal of Fluids and Structures, 27, 311-328.

Hachem, *F*., *Schleiss*, *A*. (2011b). Monitoring of steel-lined pressure shafts and tunnels. International Journal on Hydropower & Dams*,* 18(3),74-77.

Hachem, *F*. (2011c). Monitoring of steel-lined pressure shafts considering water-hammer wave signals and fluid-structure interaction. PhD thesis No 5171 (2011), Ecole Polytechnique Fédérale de Lausanne (EPFL), Switzerland.

Hachem, *F*., *Schleiss*, *A*. (2011d). Detection of local wall stiffness drop in steel-lined pressure tunnels and shafts of hydroelectric power plants using steep pressure wave excitation and wavelet decomposition. Journal of Hydraulic Engineering, DOI: 10.1061/(ASCE)HY.1943-7900.0000478.

Hachem, *F*., *Schleiss*, *A*. (2011e). The influence of drop in pipe wall stiffness on water-hammer speed and attenuation. Journal of Hydraulic Research, Accepted for publication.

Hachem, *F*., *Schleiss*, *A*. (2011f). Physical tests estimating the water-hammer wave speed in pipes and tunnels with local weak wall stiffness. Proceedings of the 2011 World Environmental & Water Resources Congress (EWRI), Palm Springs, California, May 22 – 26, 2011.

Hachem, *F*., *Schleiss*, *A*. (2011g). Monitoring of steel-lined pressure shafts using water-hammer records and wavelet filtering and decomposition. . Proceedings of the 34th IAHR Congress 2011, Brisbane, Australia, 26 June to 1 July, 2011.

Hachem, *F*., *Schleiss*, *A*. (2011h). On-line monitoring of steel-lined pressure shafts by using pressure transient signals under normal operation conditions. Journal of Hydraulic Engineering, submitted as a scientific full paper in September 2011.

Halliwell, *A*. (1963). Velocity of a waterhammer wave in an elastic pipe. *ASCE* Journal of the Hydraulics Division, 89,1-21.

Jaeger, *C*. (1977). Fluid transients in hydro-electric engineering practice. Blackie and Son Limited, Glasgow and London.

Lang, *F*. (1987). Correlation Techniques. Van Nostrand Reinhold Company, New York.

Lyons, R. (1997). Understanding digital signal processing. Addison-Wesley, USA.

Mallat, *S*. (1990). A Wavelet Tour of Signal Processing. Academic Press, San Diego, CA.

Mathworks (2008). MATLAB, Natick, Mass, www.mathworks.com.

Montgomery, *D*. (2005). Introduction to statistical quality control. John Wiley and Sons, Inc., USA, fifth edition.

Parmakian, *J*. (1963). Waterhammer analysis. Dover Publications, Inc., New York.

Shin, *K*., *Hammond*, *J*. (2008). Fundamentals of signal processing for sound and vibration engineers. John Wiley and Sons, New York.

Wylie, *E*., *Suo*, *L*. (1993). Fluid transients in systems. Prentice Hall, Fascimile Edition.

Adresse des auteurs

Fadi Hachem, *Anton Schleiss*
Laboratoire de Constructions Hydrauliques (LCH)
Ecole Polytechnique Fédérale de Lausanne (EPFL)
Station 18, CH-1015 Lausanne, tél. +41 21 693 2385
fadi.hachem@a3.epfl.ch, anton.schleiss@epfl.ch

Suivi du projet et dates clefs

Ce projet de recherche a été suivi de près par le directeur de thèse Prof. Anton Schleiss. Plusieurs séances d'organisation et de discussion ont été régulièrement organisées chaque cinq à six semaines.

Quatre présentations ont été données dans le cadre du programme de conférences internes du LCH et six autres pendant les séances techniques du consortium HydroNet I. En plus, trois rapports intermédiaires ont été soumis à l'OFEN en août 2008, août 2009 et en novembre 2010.

Ce projet de recherche a été défendu devant un jury de spécialistes le 9 septembre 2011. Le rapport de thèse intitulé: "Monitoring of Steel-lined pressure shafts considering water-hammer wave signals and fluid-structure interaction" a été accepté sans réserve par les membres de jury. Il a été déposé en version finale au service académique de l'EPFL le 19 septembre 2011. Une défense publique prévue le 28 octobre 2011 clôturera les quatre années qui ont été consacrées à ce projet.

Annexe

Publications 2011

The influence of drop in pipe wall stiffness on water-hammer speed and attenuation

HACHEM FADI E., PhD Candidate, Laboratory of Hydraulic Constructions (LCH), Ecole Polytechnique Fédérale de Lausanne (EPFL), Station 18, 1015 Lausanne, Switzerland. *E-mail:* fadi.hachem@a3.epfl.ch
SCHLEISS ANTON J., Professor and Director, Laboratory of Hydraulic Constructions (LCH), Ecole Polytechnique Fédérale de Lausanne (EPFL), Station 18, 1015 Lausanne, Switzerland. *E-mail:* anton.schleiss@epfl.ch

Abstract

In this paper the influence of local drop of wall stiffness of pressurized waterways on the pressure wave speed and wave attenuation during transients is investigated experimentally. A new signal processing procedure to identify the presence of a weak reach is introduced and validated by physical experiment tests. It is based on accessing the pressure and vibration records acquired at the both ends of a multi-reach steel test pipe. The water-hammers are generated by closing a downstream valve and the weak reaches are simulated by replacing the steel reaches with Aluminum and PVC materials. The method is also capable to locate the weakness of stiffness along the test pipe when one PVC reach is used.

Keywords: WATER-HAMMER, WAVE SPEED, WAVE ATTENUATION, STEEL-LINED PRESSURE TUNNELS, MONITORING, DROP OF WALL STIFFNESS, GEOPHONES

1 Introduction

Unsteady flows in pressurized water systems offer a challenge in computation, visualization, and analysis, particularly in presence of system facilities and features (elbows, valves, junctions, and so on). The interaction between the structural wall and the confined water influences the transient behavior of the flow and provides some signatures of specific characteristics along the conduit (Bergant *et al.*, 2008a). The changes in transient pressures generated by a wall leaking crack have been extensively studied using several hydraulic based monitoring techniques (Ferrante and Brunone, 2003, Covas *et al.*, 2005, Hunaidi, 2006). A different structural wall aspect has been studied by Stephens *et al.* (2008) to estimate the location of internal wall damage of a composite concrete-steel pipeline based on transient model combined with a Genetic Algorithm and field measurements. It is also known that a local difference of the wall characteristic impedance (function of the wave speed and the flow area) relative to the rest of the waterway system generates hydro-acoustic boundaries that create wave reflections and transmissions and change the wave speed.

The alteration of the water-hammer wave speed and wave attenuation that are induced by substituting certain reaches of the steel test pipe with others of different material (Aluminum and PVC), called “weak reaches” throughout this paper, have been investigated experimentally. Transient signals of pressure and vibration are acquired at the both ends of the pipe and then scrutinized using new processing methods. The proposed procedure can be used practically in monitoring of steel-lined pressure shafts and tunnels to identify the local deterioration of the backfill concrete or the rock zone surrounding the liner. The deteriorated multilayer system (steel–concrete–rock) that composes the wall of these structures is experimentally simulated by a weaker Aluminum or PVC reach.

2 Theoretical background

2.1 Mass and Momentum equations for one-dimensional water-hammer flows

The water-hammer phenomenon in pressurized waterways has been studied long time ago. The combined efforts of researchers have resulted in the following classical mass and momentum equations for one-dimensional water-hammer flows (Wylie and Streeter, 1993):

$$\frac{\partial q}{\partial x} + \frac{g\pi D^2}{4a^2}\frac{\partial h}{\partial t} = 0 \tag{1}$$

$$g\frac{\partial h}{\partial x} + \frac{4}{\pi D^2}\frac{\partial q}{\partial t} + \frac{4}{\rho_w D}\tau_w = 0 \tag{2}$$

in which, $q(x,t)$ is the flow discharge, $h(x,t)$ is the piezometric head, g is the gravitational acceleration, D is the internal diameter of the pipe or tunnel, a is the water-hammer wave speed, ρ_w is the water density, x is the spatial coordinate along the longitudinal axis, t is the time, and τ_w is the shear stress at the water-wall interface.

2.2 Water-hammer wave speed

The quasi-static wave speed, which means without Fluid-Structure Interaction (FSI), can be estimated from references such as Wylie and Streeter (1993). In FSI case, the wave speed becomes frequency-dependent and other mathematical model than Eqs. (1) and (2) should be used. Some of these models can be found in Lavooij and Tijsseling (1991), and Tijsseling (2007). Between the quasi-static and FSI cases, transient models similar to those proposed by Covas *et al.* (2004) consider the pipe wall as a linear-viscoelastic material.

In steel-lined pressure tunnels under plain strain conditions, linear elasticity and small deformations considering neither the FSI nor the dynamic or creep effects of the tunnel wall, the water-hammer wave speed can be estimated from the flowing formula:

$$a = \sqrt{\frac{1}{\rho_w\left(\frac{1}{K_w} + \frac{2}{r_i}\cdot\frac{\mathrm{d}u_r^s(r)}{\mathrm{d}p}\right)}} \tag{3}$$

where, $\mathrm{d}u_r^s(r)/\mathrm{d}p$ is the first derivative of the radial displacement of the steel liner u_r^s relative to the internal pressure p at the water-liner interface of radius r_i, and K_w is the bulk modulus of water. The $\mathrm{d}u_r^s(r)/\mathrm{d}p$ ratio is a constant value which depends on the geometrical and mechanical characteristics of the steel liner and on the state (cracked or uncracked) of the surrounding backfill concrete and rock mass (Hachem and Schleiss, 2011a). The bulk modulus and density of water and, thus, the wave speed are influenced by the presence of air and sediments in water. By ignoring the presence of mixed air inside the flow and by considering as basic configuration the actual state of pressure tunnel at the beginning of monitoring, the velocity of a pressure wave traveling between two cross-sections of the tunnel will be affected by the local increase of its cross-sectional area or/and the decrease of the radial stiffness of its wall. The increase of the cross-sectional area is induced by the yielding of the steel liner of low to moderate strength while the decrease of the stiffness is the consequence of a progressive deterioration of the backfill concrete and the near-field rock mass. The drop of wall stiffness can be generated in both low and high strength steel liners and can be considered as the first indicator of a possible future liner break. Therefore, a reliable and continuous estimation of the wave speed is crucial to detect the formation of weak reaches of low wall stiffness somewhere along the pressure shafts and tunnels.

2.3 Wave attenuation

The attenuation of water-hammer wave along the pressurized waterways is caused by the energy dissipation induced by many factors such as surge control devices, the presence of dissolved air in water, the shear stress effect and the inelastic behavior of the pipe or shaft wall, leakage and FSI (Bergant *et al.*, 2008a and 2008b). The inelastic behavior is important in plastic pipes and it is related to the mechanical properties of the pipe wall and to the fluid wave frequency (Hachem and Schleiss, 2011a). The wall shear stress, τ_w, is the summation of a quasi-steady and an unsteady friction component. The former is estimated using expressions such as the Darcy-Weisbach and Hazen-Williams formulae and the latter is obtained from empirical-based models such in Bergant *et al*. (2001) or from physically-based models such in Vardy *et al*.

(1993). The wave dissipation due to steady or unsteady friction becomes important in case of high friction factor or very long pipelines with small internal diameter (Ghidaoui *et al.*, 2005).

The attenuation of water-hammer wave can also be induced by the wave transmission and reflection phenomena encountered at the boundaries of the weak reaches. This boundaries effect alters particularly the front of the wave crossing such reaches. For a frictionless liner wall, the incident wave will have a magnitude, at the n^{th} boundaries of the weak reaches, equal to (Wylie and Streeter, 1993)

$$\frac{h_n - h_0}{h_w - h_0} = 2^n \prod_{j=1}^{n} \frac{1}{1 + a_{j+1} A_j / a_j \ A_{j+1}} \tag{4}$$

where, h_n is the magnitude of the transmitted wave crossing the n^{th} boundary, h_w is the magnitude of the incident wave before reaching the weak reach, h_0 is the steady state piezometric head, A_{j+1} and A_j are the cross-section area and a_{j+1} and a_j are the wave speeds in reaches (j+1) and (j), respectively. Therefore, the formation of a weak reach somewhere along pressure shafts and tunnels induces additional attenuation of pressure waves due to the higher damping coefficient of the weak reach wall and the wave reflection/transmission at its boundaries. In this paper, the latter attenuation type is discussed and it will be considered as the second indicator of the existence of a weak reach along the shafts or tunnels.

3 Experimental tests

3.1 Set-up description

The experimental facility, shown in Fig. 1, is a close hydraulic loop designed to generate water-hammer transients inside a multi-reach steel test pipe that has an internal diameter of 150 mm and a length of 6.25 m measured from the shut-off valve to the upstream air vessel. The shut-off valve is followed by a purge valve, two elbows, an elastic joint and a control valve located at the entrance of the supply reservoir. The total length of the test pipe comprising all these pieces is about 2 m. The test pipe is divided into several reaches of 0.5 m and 1.0 m length fitted together with flanges having an external diameter of 285 mm and a thickness of 24 mm. The flanges are also used to rigidly fix the test pipe along its length in order to minimize any longitudinal and transversal movements during the tests. The weak reaches are modeled by using pipe wall materials having different ($E \cdot e$) values than the rest of the test pipe where E is the Young modulus and e is the thickness of the pipe wall. Aluminum and PVC reaches of $E \cdot e$=345 MN/m and 15 MN/m, respectively, have been used. This consists of a local drop of stiffness of the pipe wall relative to steel ($E \cdot e$=945 MN/m) of about

63% in the Aluminum case and near 98% in the PVC case. A total number of 120 tests have been carried out on the ten test pipe configurations that are shown in Fig. 2. For each configuration, 12 repetitive tests have been performed. An initial steady-state flow around 65 l/s (flow velocity inside the test pipe = 3.7 m/s, and Reynolds number = 462,500) and a mean pressure of 0.21 bar were maintained constant for all tests. The water-hammer was generated by closing the downstream guillotine valve which is activated by an air jack equipped with an input and output air electro-valves. The mean closure time of this valve was around 0.235 s which is considered slow relative to the characteristic time of the test pipe equal to 0.013 s. The volume of air needed to activate the jack is provided by an air compressor with a constant pressure of 10 bars. The opened and closed states of the shut-off valve are detected by two infrared diffuse sensors. On the highest point of this conduit, an air purge valve is installed to evacuate the captured air inside the test rig. The data acquisition system includes: (i) eight pressure transducers (HKM-375M-7-BAR-A, Kulite) with a pressure range of ±7 bars and an accuracy of 0.5%, (ii) two geophones (SM-6/S-B, 4.5 Hz, 3500 ohm, SENSOR Nederland b.v.) with a sensitivity of 78.9 V/(m/s) and a tolerance of ± 5 %, (iii) a NI-USB-6259 acquisition card M series with 32 analogue input channels and 2 analogue output channels to activate the two electro-valves of the shut-off valve, and (iv) a personal computer. The water-hammer pressures P1 and P2, and the output geophones signals V1 and V2, were recorded at sections S1 and S2 situated at the both ends of the test pipe (Fig. 1) at a sampling frequency f_s = 20 kHz.

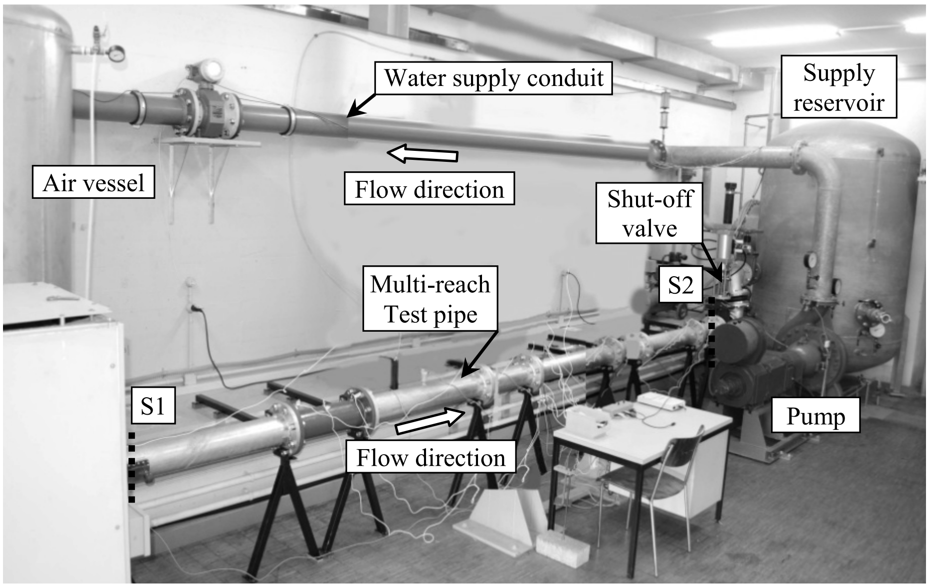

Fig. 1 Global view of the experimental facility

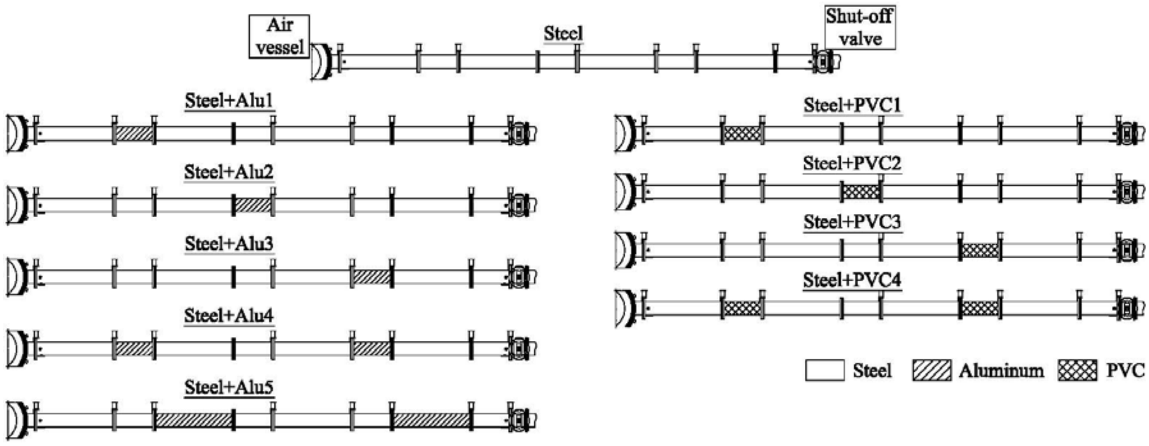

Fig. 2 The ten different configurations of the test pipe

3.2 Data analysis

3.2.1 Estimation of the wave speed based on pressure data

The wave speed is estimated by processing the water-hammer pressure and the radial vibration of the pipe wall at sections S1 and S2. Typical time histories of normalized pressures and geophones outputs are shown in Figs. 3a and 3b. The pressure signals inside the window W1 are generated at the beginning of the valve closure by the external pressure excitation caused by the impact of the air inside the jack of the valve. These pressure fluctuations die out after 0.045 s from the beginning of the valve closure. This defines the lower time border of a second window, W2, in which the progressive stoppage of the flow by the valve generates water-hammer pulsations inside the test pipe. The upper time border of W2 was fixed after 0.16 s from the start of the valve closure. Beyond this time, a series of no flow tests has revealed the presence of an important pressure drop followed by high-amplitude and high-frequency fluctuations. The former is probably caused by the compression and expansion of an air pocket inside the upper cover of the valve whereas the latter is perhaps generated by the deformation, friction and vibration of the internal core of the valve. The pressure signals of 0.12 s length acquired within the window W1 have been analyzed in Hachem and Schleiss (2010, 2011b) where a new method for detecting the presence, location and severity of the local weak reach has been proposed. The pressure signals inside the window W2 do not have a clear wave front that can be easily identified and followed as in their first parts. Therefore, a new procedure to estimate the wave speed from the pressure records inside W2 is proposed in this paper. It is validated by a series of experimental tests.

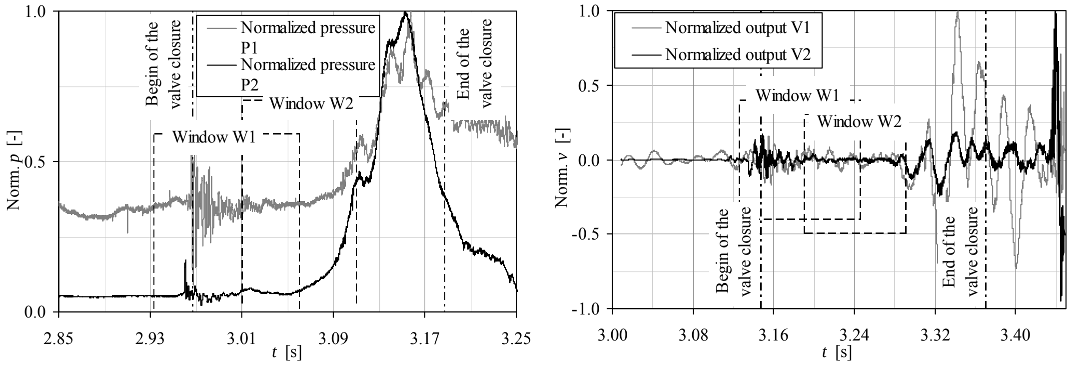

(a) (b)

Fig. 3 Typical records of the measured transient records at upstream and downstream sections S1 and S2: (a) pressures and (b) geophones outputs

This procedure starts with decomposing each signal P1 and P2 into an approximation (A_J) and several details (D_i) components using the wavelet decomposition technique (Mallat, 1990, Hachem and Schleiss, 2011b, and Ferrante and Brunone, 2003). The Daubechies (db10) mother wavelet is used. The details D_4 to D_7 for each pressure signal are then summed together to construct two new signals S(P1) and S(P2). This construction filters the signals with a band-pass filter of low and high frequencies of 72 and 486 Hz, respectively. These frequencies are chosen to preserve the information of the incident-reflection waves between the supply reservoir and the air vessel ($= a_{steel} / (2 \cdot L_{max}) = 1{,}245.4/(2 \cdot 8.25) = 75.5$ Hz), and between the closest weak reach boundary to the air vessel and this latter ($= a_{steel} / (2 \cdot L_{min}) = 1{,}245.4/(2 \cdot 1.29) = 482$ Hz). The signals S(P1) and S(P2) of the pressure records given in Fig. 3a are shown in Fig. 4a.

The procedure continues with the computation of the energy content history of signal S(P2) using the floating Root Mean Square (RMS). In this paper, the RMS method is applied by using the following equation:

$$\mathrm{RMS}_j = \sqrt{\frac{1}{N}\sum_{i=j}^{j+N-1} p_i^2} \quad (5)$$

in which, p_i is the discrete pressure values of the signal S(P2), and N is a real parameter that defines the resolution of the RMS and represents the number of pressure points inside a one period interval. The high-frequency, f_{max}=500 Hz is used to determine the value of N according to the formula: $N = (1/f_{max}) \cdot f_s = (1/500) \cdot 20{,}000 = 40$. The RMS curve shows positive shifts at times when an important pressure energy package crosses the measurement section S2. A RMS threshold line of 0.01 bar was chosen to define a portion or a signature of the S(P2) signal. This signature is limited by the times of the two minimum peaks of the first RMS lobe that has a positive shift that crosses the threshold line. The RMS curve, the energy threshold line, and the signal borders of the S(P2) pressure records given in Fig. 3a are shown on Fig. 4b.

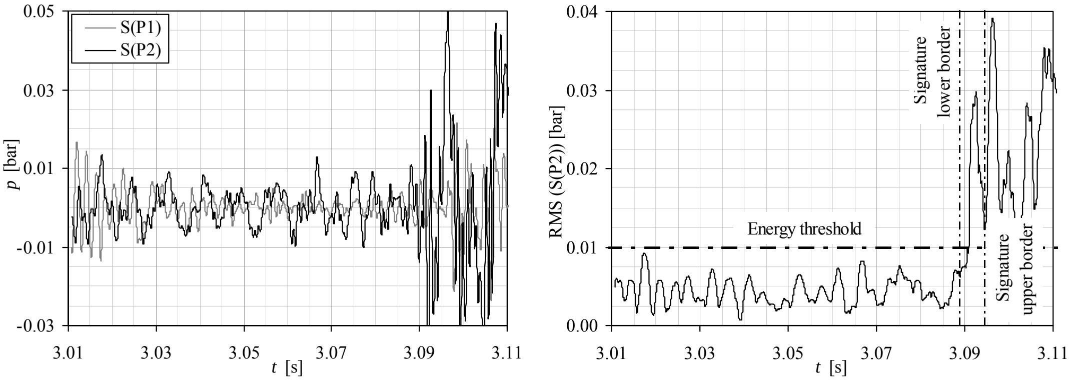

(a) (b)

Fig. 4 (a) Pressure signals constructed by summing the wavelet details from D_4 to D_7 and (b) the floating Root Mean Square of the S(P2) signal shown in (a) including the energy threshold line and the borders of the S(P2) pressure signature

The procedure ends with a cross-correlation between the signature of pressure S(P2) and the pressure S(P1). For discrete functions, the cross-correlation is defined as follows (Lang, 1987):

$$\left(\mathrm{S(P1)} * \mathrm{S(P2)}\right)[n] = \sum_{m=l}^{s} \mathrm{S(P1)}^{*}[m] \cdot \mathrm{S(P2)}[n+m] \tag{6}$$

where, $\mathrm{S(P1)}^{*}$ is the complex conjugate of S(P1), l and s are the lower and upper limits of the signal time interval, respectively, and n and m are two positive integers. The estimated travel-time of the water-hammer wave speed between the two measurement sections S1 and S2 corresponds to the time-lag at the maximum positive peak of the cross-correlation curve identified between two time borders obtained from the logical wave speed values of 1,400 and 800 m/s according to the relations: $t_{\text{Lower border}}$ = 5.88/1,400 = 0.0042 s, $t_{\text{Higher border}}$ = 5.88/800 = 0.00735 s. The peak time, $t_{\mathrm{P2,P1}}$, of the signals given in Fig. 4a is equal to 0.0059 s and can be easily transformed to wave speed according to the formula:

$$a = \frac{L_{\mathrm{P2,P1}}}{t_{\mathrm{P2,P1}}} \tag{7}$$

where, $L_{\mathrm{P2,P1}}$ is the known distance of 5.88 m separating the two pressure sensors P1 and P2.

The estimated values of the wave speed between sections S1 and S2 determined according to the procedure in Hachem and Schleiss (2011b) for pressure signals in window W1 and those obtained according to the procedure described in this paper for signals in window W2, are compared in Figs. 5a and

5b, respectively. These wave speeds are given for all the 120 tests that have been carried out on the ten configurations of the test pipe. The means and standard deviations of each 12 tests that correspond to each pipe configuration are also shown. A very good agreement is found between mean values estimated by the two pressure based methods with a maximum relative difference of 5.8% for the configuration “Steel+PVC4”.

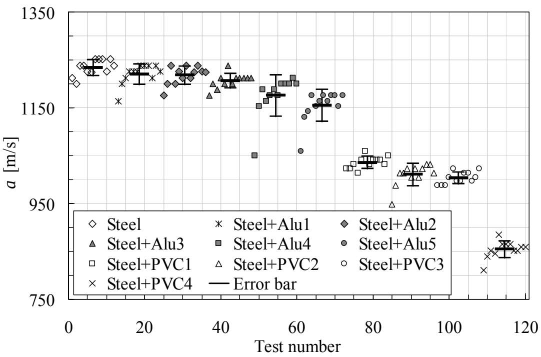

(a)

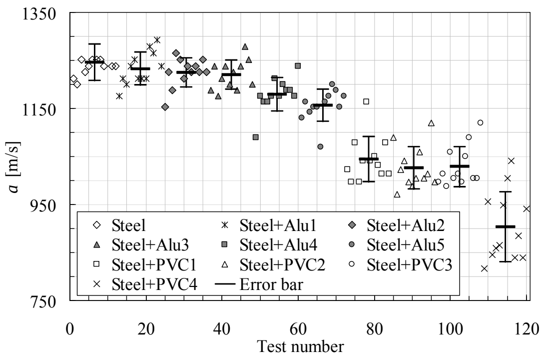

(b)

Fig. 5 Water-hammer wave speed estimated from the pressure records: (a) in case of steep wave front as shown in window W1 of Fig. 3a, (b) in case of waves generated by the progressive stoppage of flow by the shut-off valve (inside the window W2 of Fig. 3b)

3.2.2 Estimation of the wave speed based on geophone data

The radial vibrations of the pipe wall were determined from the measurement of the two geophones fixed on the exterior surface of the test pipe at sections S1 and S2. The geophone is a simple sensor that has a suspended moving coil around a permanent magnet. When the coil moves relative to the magnet, a voltage is induced in the coil according to Faraday law. The induced voltage is proportional to the relative coil-magnet velocity and the proportionality factor is known as the sensitivity *G*. This type of sensors is cheap, passive (no need for power supply), and has good linearity. It is usually used in seismologic survey to detect refraction and/or reflection from subsurface formations after generating a surface disturbance by explosives or other means. It has been also used in leak detection monitoring of shallow underground pipelines by allowing users to scan the entire length of the inspected pipelines and to hear the noise coming up from the leak (Mays, 2000). Hunaidi (2006) developed an acoustic method based on cross-correlating two accelerometer signals to determine the wave speed in a water distribution pipe reach in purpose to extract its mean wall thickness from standard theoretical wave speed formulae. The advantage of the method developed herein consists of using geophones instead of relatively expensive accelerometers and signal conditioning hardware. The wave speed values obtained from processing the geophone output signals V1 and V2 measured inside window W1 (Fig. 3b) are compared to those estimated from pressure signals.

The analysis starts by decomposing the two geophone signals using the Daubechies (db10) mother wavelet. Figure 6a shows the time history of the detail D_4 for the geophone output V2 given in Fig. 3b. It shows a significant amplitude increase at time t_{2max} when the wave front crosses the pipe section S2. This signal detail is transformed to pipe surface displacement, u, according to the following transfer function, $H(f)$, obtained from the second order differential equation of motion of the damped mass of the geophone sensor:

$$H(f) = \frac{\mathrm{FFT}(v[\mathrm{Volts}])}{\mathrm{FFT}(u[\mathrm{m}])} = \frac{-2\pi \mathrm{i}\, f^3 G}{f_0^2 - f^2 + 2\mathrm{i}\xi f_0 f} \tag{8}$$

where, FFT is the Fast Fourier Transform, v is the geophone output signal in Volts, i is the complex number $(-1)^{1/2}$, f is the frequency, and f_0 (= 4.5 Hz) and ξ (=0.58) are the natural frequency and damping ratio of the geophone, respectively. The maximal computed radial displacement at time t_{2max} is compared to the theoretical radial displacement of the pipe wall determined from the pipe formula that uses the pipe wall characteristics at section S2 and the pressure increase value at the wave front. This comparison shows a relative mean error around 12% and proves that detail D_4 contains the most important part of the radial component of the pipe wall displacement. At section S1, the summation of details D_4 and D_5 was considered to identify the arrival time, t_{1max}, of the water-hammer pressure wave (Fig. 6b). The time t_{1max} is determined from the first peak time of record (D_4+D_5) that gives a wave speed value between 800 and 1,400 m/s. The wave speed is computed according to Eq. (7) with $t_{P2,P1}$ = (t_{1max} - t_{2max}). The comparison between the wave speeds estimated by the proposed geophone based method and pressure approach for the five configurations of the test pipe shows good agreement between the two methods with a maximum relative difference of 9.3%. The wave speeds obtained from the geophone signals for the “Steel” configuration are around 80 m/s higher than those estimated from pressure measurements. The discrepancy in water hammer wave speed in case of “Steel” configuration is probably caused by the interference of geophones with the stress waves traveling at high speed inside the test pipe wall. These waves are considerably attenuated by the presence of the PVC reach along the pipe. It should be mentioned here that the geophones signals inside the window W2 could not be analyzed by the herein proposed method due to the long dissipation time of the output signal generated in window W1.

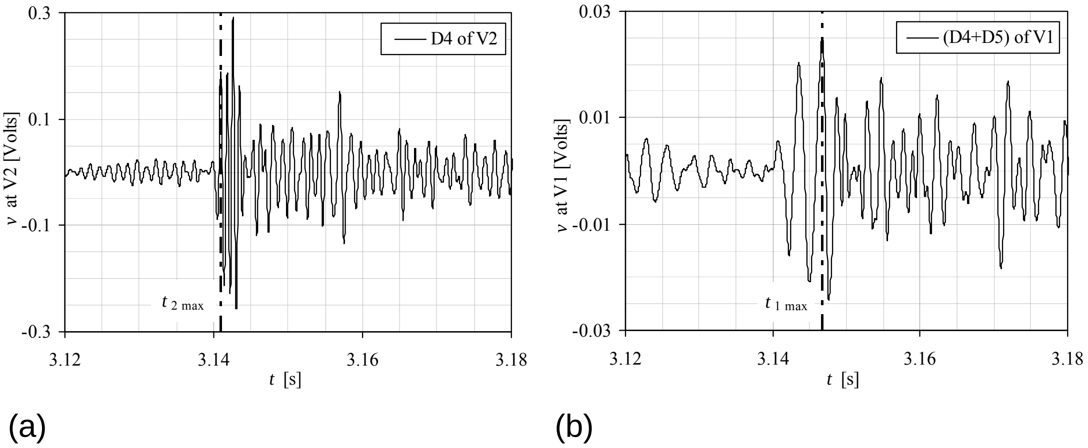

Fig. 6 The wavelet details components of the geophones output signals shown in window W1 of Fig. 3b: (a) D_4 at section S2, (b) (D_4+D_5) at section S1

3.2.3 Estimation of the wave attenuation factor induced by the transmission/reflection phenomena at the weak reach boundaries

For the front wave generated in window W1, a total number of six pressure sensors were used to measure the water transient inside and at the upstream and downstream sides of the Aluminum and PVC reaches. Three sensors were placed inside the weak reach (one in the middle and two at 60 mm from each of its end), one upstream and two downstream from it (Fig. 7a). For each "Steel+PVC" and "Steel+Alu" configuration, the six sensors were displaced to follow the position of the weak reach along the pipe. The pressure sensors at sections S1 and S2 were used to record the global wave attenuation along the test pipe. Figure 7a gives the theoretical and measured pressure head ratios between the transmitted and incident waves, as it is defined in Eq. (4), for three different reaches made of steel, Aluminum, and PVC materials.

In presence of PVC reach, the measured results show that the front wave looses around 44% of its magnitude when it enters the weak reach. The reflection coming back from the downstream border amplifies the wave front by about 32% (Fig. 7b). The wave continues its downstream propagation with a attenuation slope higher than in Steel and Aluminum cases. The measured ratios inside the weak reach are 20% higher than the theoretical values obtained from Eq. (4). The higher downstream slope and the difference between the theoretical and measured pressure ratios are probably caused by the inelastic behavior of the PVC reach. For the Aluminum reach, the same wave behavior is observed with less attenuation and less amplification when entering and leaving the reach, respectively. The additional wave attenuation induced by the Aluminum and PVC reaches is confirmed by the measurement of the total attenuation factor of the entire test pipe.

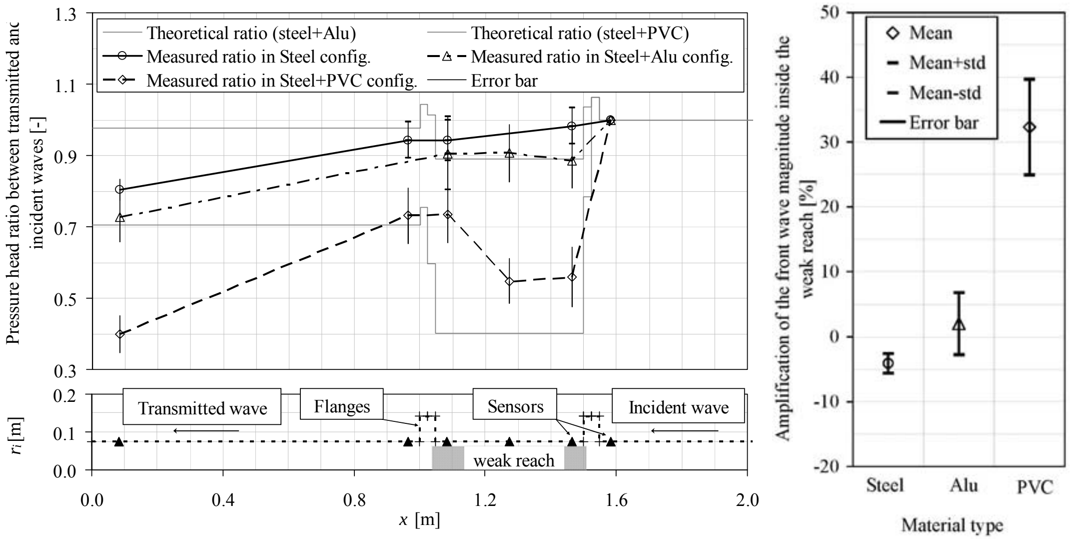

(a) (b)

Fig. 7 (a) Local theoretical and experimental attenuation ratios of the pressure wave front encountered by the weak reach, (b) means and standard deviations of the amplifications of the wave front magnitude inside the weak reach for different materials types

Figure 8 shows the relative attenuation ratios between S1 and S2 for all the test pipe configurations. Significant and proportional differences (+20% in "Steel+PVC1,2,3" and +35% in "Steel+PVC3") between the "Steel" and the "Steel+PVCs" configurations can be observed. Such differences cannot be identified in the "Steel+Alu" cases. It should be mentioned here that it was difficult to extract similar information regarding the wave attenuation by using the geophones or the pressure records situated within window W2.

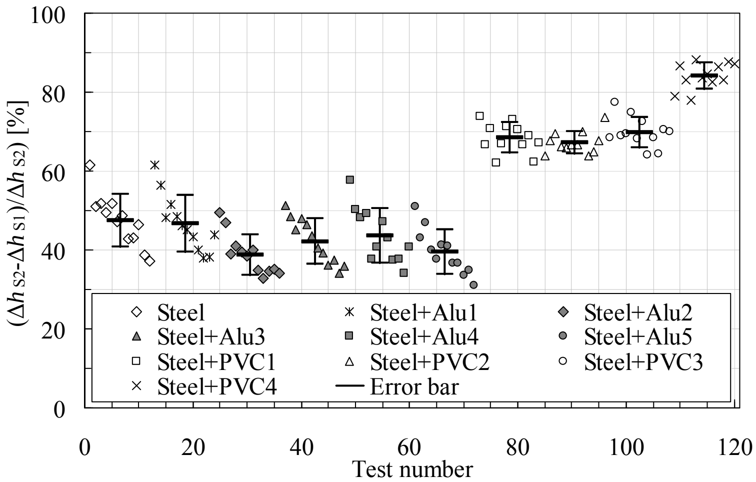

Fig. 8 Relative attenuation ratios between measurement sections S1 and S2 estimated from the pressure records having a steep wave front

3.2.4 Weak reach location

The incident–reflection travel times between the weak reach and the air vessel are estimated using the Fast Fourier Transform (FFT) of the pressure records inside the Window W2. The FFT records of the test configurations with Aluminum reach are very similar to those for “Steel” configuration. This is due to the small magnitude of the wave that is reflected backwards from the Aluminum reach boundaries. Therefore, the localization of such reaches using the FFTs approach is not possible. For each “Steel+PVC” test pipe configuration, the mean of the normalized FFT (with Hanning windowing) at S1 and S2 is computed. The normalization is obtained by dividing the FFT magnitudes by the one at 80 Hz. This frequency corresponds to the incident-reflection travel time between the supply reservoir and the air vessel. Figure 9 depicts the average curves of the normalized FFT for P1 and P2 signals acquired from the “Steel” and “Steel+PVCs” configurations. The curves of “Steel+PVCs” show significant differences in their pattern compared to the “Steel” configuration. These differences are induced by the pressure reflection generated by the weak reach inside the test pipe. The frequency that corresponds to the weak reach for each pipe configuration is identified after discarding the FFT peaks of the “Steel+PVCs” records that have the same frequencies as peaks of the “Steel” configuration (see the grey bands shown in Fig. 9). For “Steel+PVC1” configuration, one of the many P1 FFT peaks (marked by circles in Fig. 9) should be chosen. This is done by using couples of P1 and P2 peak frequencies to compute the fundamental frequency of the test pipe, f_{fund} , according to the following equation:

$$f_{fund} = \frac{f_{\max,P1} \cdot f_{\max,P2}}{f_{\max,P1} + f_{\max,P2}} \qquad (9)$$

where $f_{\text{max,P1}}$ and $f_{\text{max,P2}}$ are the FFT maximum peaks of P1 and P2, respectively. The frequencies f_{fund} are then compared to the theoretical value a_{steel} / ($2 \cdot L_{\text{max}}$) = 75.5 Hz. The pair of frequencies which gives the nearest f_{fund} relative to the theoretical value is retained. For “Steel+PVC1” configuration, these frequencies are $f_{\text{max,P1}}$ = 320 Hz and $f_{\text{max,P2}}$ = 120 Hz. For “Steel+PVC2” and “Steel+PVC3” configurations, the only remaining frequencies of the FFT P1 records after discarding peak frequencies of the “Steel” configuration are 210 and 140 Hz, respectively. For these configurations, Eq. (9) has not been used to identify the frequency peaks.

The estimation of the incident-reflection travel distance, L_1 between the weak reach and the air vessel is done by using the mean wave speed of the “Steel” configuration (a_{steel}=1,245.4 m/s) and the identified fundamental frequencies from the FFT of P1. The travel distances and the errors relative to the real path lengths are presented in Table 1. The error in estimating the position of the weak reach relative to the real position of its middle section varies from 2.3% to

22.7%. Fig. 10 is the flow chart represented by the step-by-step procedure of the analysis procedure used for the physical tests.

Table 1 Estimated distances between the middle of the weak reach and sensor P1 obtained from the FFT approach for the three test pipe configurations “Steel+PVC1,2,3”

Test pipe configuration	Path	Real path length to the middel of the WR, L_1	Estimated wave speed for “Steel” configuration	P1 peak frequency $f_{max,P1}$	Estimated L_1 path length	Relative error
		[m]	[m/s]	[Hz]	[m]	[%]
Steel+PVC1	P1-WR*	1.54		330	1.89	22.7
Steel+PVC2	P1-WR	3.04	1,245.4	210	2.97	2.3
Steel+PVC3	P1-WR	4.56		140	4.45	2.4

* *WR stands for Weak Reach*

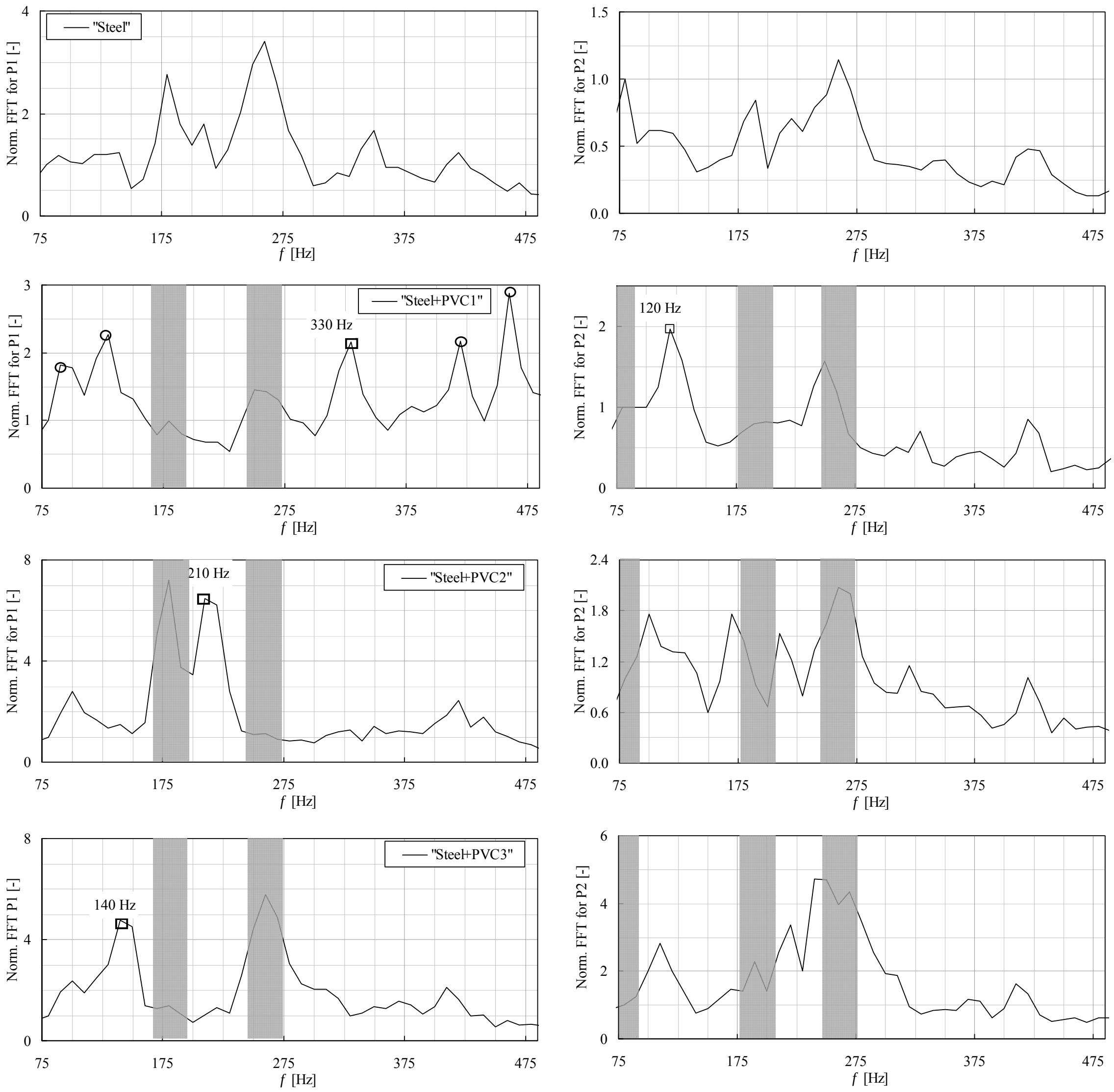

Fig. 9 The normalized Fast Fourier Transforms of pressures P1 and P2 situated inside the Window W2 of Fig. 3a for the “Steel” and “Steel+PVCs” test pipe configurations

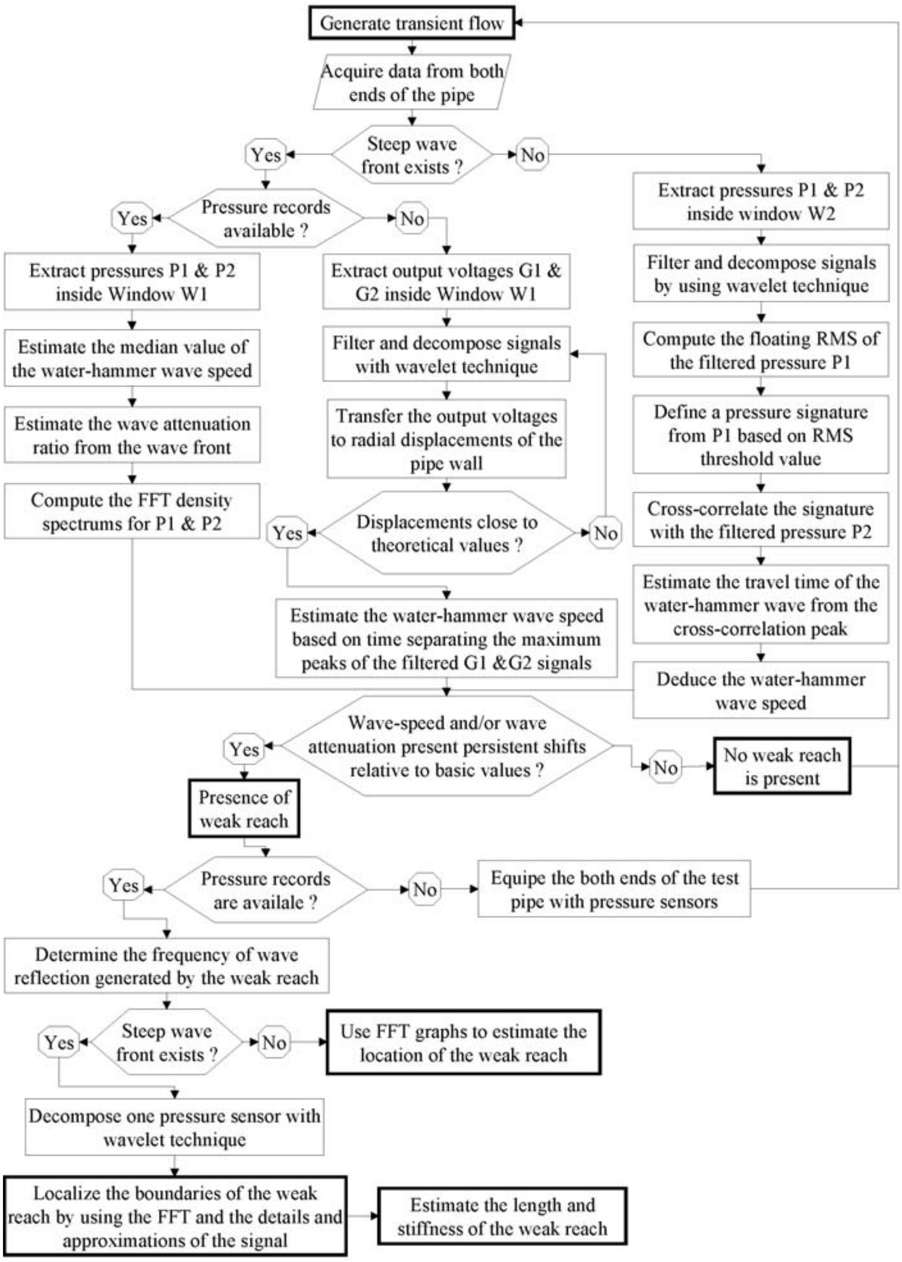

Fig. 10 Flow chart of the monitoring procedure applied to the experimental facility

4 Conclusions

A new procedure for estimating the wave speed and the wave attenuation inside pressurised waterways during water-hammer phenomena in presence of local drop of wall stiffness was proposed. This procedure was validated by a series of 120 experimental tests that have been carried out in a multi-reach steel pipe where the weak reaches were physically modelled by exchanging the steel reaches by Aluminum and PVC materials. It is based on acquiring and processing pressure and vibration records obtained at two sections of the test pipe. This method can also estimate the position of the weak reach when only one PVC reach is used. It includes the wavelet decomposition and filtering techniques and the Fast Fourier Transforms. The following points may be concluded:

i. The wave speeds computed by using the proposed procedure from both the pressure and geophone sensors are in very good agreement with those obtained from pressure records in previous tests (Hachem and Schleiss, 2011b) using steep waves fronts. A maximum relative mean error of 5.8% was observed in the “Steel+PVC4” configuration when the pressure records are used to estimate the wave speed. The processing of the geophone signals give approximately the same mean error but overestimate the wave speed values in “Steel” configuration by about 80 m/s.
ii. The method was able to evaluate the wave attenuation factor by using only the steep front wave pressures. Significant and proportional attenuation differences of +20% in “Steel+PVC1,2,3” and +35% in “Steel+PVC4” relative to the “Steel” configuration have been observed.
iii. The wave speed and wave attenuation factor during transients can be considered as global indicators of local and large changes in stiffness (stiffness decreases down to 98%) of the pipe wall.
iv. By using the FFT analysis for the pressure signals it was possible to localize one weak reach that has a very low stiffness (PVC reach) relative to the steel. The error in estimating the position of such reach relative to the real position of its middle varies from 2.3% to 22.7%.

The monitoring procedure consists on acquiring continuously the transient pressure signals and calculating the wave speed. Once a significant and persistent decrease of the wave speed value and increase of the wave attenuation are detected, a drop of the wall stiffness is suspected to be occurred somewhere along the shaft. The pressure FFTs should reveal a new peak at a frequency that corresponds to reflections from the weak reach. If the transient signal is steep enough, the Wavelets approach is then used to locate the weakness and to estimate its severity. The state of the shaft with weak reach will be then considered as the basic configuration for the future monitoring records. The reflections coming from other irregularities such as galleries and caverns near the tunnel and from partially closed valves can easily be discarded due to their known locations. The air pocket sources have a different pressure print out than the gradual drop of wall stiffness. They are characterized by a drastic and scattered drop of the wave speed. The roughness increase due to corrosion of the liner is expected to have minor effect and the blockages are very improbable to occur in this type of conveying waterways of large diameter. Finally, leaks have a special wave print which is characterized by very steep front reflections that cannot be identified by the FFT approach and thus do not affect the accuracy of the method. The absence of pipe joints (as in case of water distribution pipelines) in the steel-lined pressure shafts and tunnels reduces the risk of important water leakage relative to the main discharge inside these structures.

In an ongoing research, the practical application of the proposed method will be tested through a series of in-situ measurements carried out on the pressure shaft of a pumped-storage power plant in Switzerland (Hachem and Schleiss, 2011c). These measurements use dynamic pressure and geophones sensors placed at both ends of the pressure shaft. They will give additional information about the steepness, energy and attenuation of water-hammer waves generated during start-up and shut-down of pumps and turbines.

Acknowledgments

The study is part of the research project *HydroNet* for the design, manufacture and operation of pumped storage plants funded by the *Swiss Competence Center Energy and Mobility* (CCEM-CH), the *Swiss Electrical Research* and the *Swiss Office for Energy*. The authors wish to acknowledge the financial support of *Lombardi Foundation* and to thank Mrs. Didia Covas for her valuable comments during her stay at LCH-EPFL as invited professor.

Notation

a	=	Water-hammer wave speed
A	=	Internal cross-sectional area of the pipe or the steel liner
D	=	Internal diameter of the pipe or tunnel
e	=	Pipe or steel liner wall thickness
E	=	Elasticity modulus
f	=	Frequency
f_0	=	Natural frequency of the geophone
f_s	=	Sampling frequency
G	=	Geophone sensitivity
h	=	Piezometric head
h_0	=	Steady-state piezometric head
h_w	=	Piezometric head of the incident pressure wave
h_n	=	Piezometric head of the transmitted pressure wave crossing the n^{th} boundary
H	=	Transfer function of the geophone sensor
K_w	=	Bulk modulus of water
L	=	Length of the pipe, tunnel or shaft
p	=	Internal water pressure
p_i	=	i^{th} discrete pressure values of the measured signal
q	=	Flow discharge
r_i	=	Internal radius of the pipe or the steel liner

t = Time
u_r^s = Radial displacement of the steel liner
v = Geophone output signal
v_0 = Steady-state flow velocity
ρ_w = Water density
τ_w = Shear stress at the water-wall interface
ξ = Damping ratio of the geophone

References

Bergant, A., Simpson, A.R., Vitkovsky, J. (2001). Developments in unsteady pipe low friction modeling. *Journal of Hydraulic Research* 39(3), 249-257.

Bergant, A., Tijsseling, A., Vitkovsky, J., Covas, D., Simpson, A., Lambert, M. (2008a). Parameters affecting water-hammer wave attenuation, shape and timing—Part 1: Mathematical tools. *Journal of Hydraulic Research*, 46(3), 373–381.

Bergant, A., Tijsseling, A., Vitkovsky, J., Covas, D., Simpson, A., Lambert, M. (2008b). Parameters affecting water-hammer wave attenuation, shape and timing—Part 2: Case studies. *Journal of Hydraulic Research*, 46(3), 382–391.

Covas, D., Stoianov, I., Mano, J.F., Ramos, H., Graham, N., Maksimovic, C. (2004). The dynamic effect of pipe-wall viscoelasticity in hydraulic transients. Part I – experimental analysis and creep characterization. *Journal of Hydraulic Engineering*, 42(5), 516–530.

Covas, D., Ramos, H., Betâmio de Almeida, A. (2005). Standing wave difference method for leak detection in pipeline systems. *Journal of Hydraulic Engineering*, 131(12), 1106–1116.

Ferrante, M., Brunone, B. (2003). Pipe system diagnosis and leak detection by unsteady-state tests. 2. Wavelet analysis. *Advances in Water Resources* 26, 107–116.

Ghidaoui, M., Zhao, M., Axworthy, D.H., McInnis, D.A. (2005). A review of water hammer theory and practice. *Applied Mechanics Reviews* 58(1-6), 49-75.

Hachem, F., Schleiss, A. (2010). Influence of local stiffness of conduits on water hammer propagation signal. *Proceedings of the First European IAHR Congress*, Edinburgh, 2010. www.iahr.net.

Hachem, F., Schleiss, A. (2011a). A review of wave celerity in frictionless and axisymmetrical stel-lined pressure tunnel. *Journal of Fluids and Structures* 27, 311-328.

Hachem, F., Schleiss, A. (2011b). Detection of local wall stiffness drop in steel-lined pressure tunnels and shafts of hydroelectric power plants using steep pressure wave excitation and wavelet decomposition. *Journal of Hydraulic Engineering*, DOI: 10.1061/(ASCE)HY.1943-7900.0000478.

Hachem, F., Schleiss, A. (2011c). Monitoring of steel-lined pressure shafts and tunnels considering water-hammer wave signal and Fluid-Structure. PhD thesis No 5171, Ecole Polytechnique Fédérale de Lausanne (EPFL), Switzerland.

Hunaidi, O. (2006). A new system for locating leaks in urban water distribution pipes. *Management of Environmental Quality: An International Journal* 17(4), 450-466.

Lang, F.H. (1987). *Correlation Techniques*. D. Van Nostrand, N J.

Lavooij, C.S.W., Tijsseling, A.S. (1991). Fluid-Structure Interaction in liquid-filled piping systems. *Journal of Fluids and Structures* 5, 573-595.

Mallat, S.G. (1990). *A Wavelet Tour of Signal Processing*. Academic Press, San Diego, CA.

Mays, L.W. (2000). *Water distribution systems handbook*. McGraw-Hill.

Stephens, M.L., Simpson, A.R., Lambert, M.F. (2008). Internal wall condition assessment for water pipelines using inverse transient analysis. *Proceedings of the 10th Annual Symposium on Water Distribution Systems Analysis*, ASCE, Kruger National Park, South Africa.

Tijsseling, A.S. (2007). Water hammer with Fluid-Structure Interaction in thick-walled pipes. *Computer and Structures* 85, 844-851.

Vardy, A.E., Hwang, K.L., Brown, J.M.B. (1993). A weighting model of transient turbulent pipe friction. *Journal of Hydraulic Research* 31, 533-548.

Wylie, E.B., Suo, L., Streeter, V.L. (1993). *Fluid Transients in Systems*. Prentice Hall, Fascimile Edition.

MONITORING OF STEEL-LINED PRESSURE SHAFTS AND TUNNELS

Fadi E. Hachem[1] and Anton J. Schleiss[2]

Abstract: A new non-intrusive monitoring method to detect the local drop of wall stiffness of the shafts and tunnels of hydroelectric power plant is presented. This method assess the water hammer pressure signals using the FFT and Wavelets transforms to extract wave reflections induced by weak reaches. The experimental facility used to validate the method with some tests results is also presented. These results show that in low dissipative media, a weak reach having an elasticity modulus not higher than 10% compared to the other part of the structure may be located by using this method. In-situ dynamic pressure measurement and analyzing are now in progress to study the possible extension of the monitoring method to real scale hydropower plants.

1 INTRODUCTION

The nowadays European electricity market offers an excellent opportunity to Swiss hydropower producers to increase their daily peak energy production. In addition to its attractive market price, such energy is essential to avoid blackouts that may cover large areas and cause important economical losses. Switzerland has developed 85% of its economically feasible hydro electrical potential [Schleiss, 2000[1]] to meet approximately 55% of the country's electricity requirements. The federal government wants to promote the future use of hydropower to a greater extent to maintain and increase the strong position of Switzerland in peak hydropower production and the exportation of high value technology. The project consortium *HydroNet*, built in 2007 and co-financed by *CCEM*[2] and *swisselectric research*[3], aims to converge towards a consistent standardized methodology for design, manufacturing, operation, monitoring and control of pumped storage power plants. One of the civil engineering field involved in this research consortium concerns the design of pressure shafts and tunnels. This paper gives an overview on the actual state of the ongoing work in this

[1] Researcher-Assistant, Laboratory of Hydraulic Constructions (LCH-EPFL), Ecole Polytechnique Fédérale de Lausanne, Station 18, 1015 Lausanne, Switzerland.

[2] Professor and Director, Laboratory of Hydraulic Constructions (LCH-EPFL), Ecole Polytechnique Fédérale de Lausanne, Station 18, 1015 Lausanne, Switzerland.

field by focusing on a new monitoring method that uses the water hammer wave signal and the fluid-structure interaction phenomenon. It includes a short state-of-the-art-review, the description of the physical scaled model with some tests results, as well as the presentation of an in-situ measurement system that acquire pressure records from the shaft of a pumped storage power plant in the Swiss Alps.

2 STATE-OF-THE-ART-REVIEW

The actual design criteria and methods for load sharing calculations for steel lined pressure tunnels and shafts have been reviewed and discussed in Hachem and Schleiss [2009[4]]. A review of wave celerity in frictionless and axisymmetrical steel-lined pressure tunnels has also been discussed in Hachem and Schleiss [2011[5]]. In this latter paper, general applicable approaches for estimating the quasi-static and frequency-dependent water-hammer-wave speed in steel-lined pressure tunnels were analyzed. The external constraints and assumptions of these approaches were discussed and the reformulated formulae were compared to commonly used expressions. An enhanced theoretical model for the steel-liner has been proposed as a basis of future development including the application of fracture mechanics to assess the response of high-strength steel which is used as lining for shafts of new hydropower plants.

The monitoring of existing steel-lined shafts and tunnels is done normally by using pressure sensors, water level measurements, and downstream and upstream flow meters. The water pressure records are usually used to check the amplitude of the transient pressures relative to a critical operation value defined during the design phase. No further advanced analyses and pressure signal processing is done. When a liner failure occurs, the water flow discharge increases and exceeds a predefined threshold. The security shut-off valve at the upstream end of the shaft closes automatically to limit the quantity of water leaking out from the shaft towards the rock surface. Nevertheless, catastrophic consequences can occur because of the important leakage volume combined with hydraulic jacking of the rock mass. Any further and additional investigation of the steel-liner regarding excessive local deformations and steel yielding requires the interruption of operation and the dewatering of the shaft for visual checking. Furthermore, no information can be easily obtained regarding the stiffness of the backfill concrete and rock mass surrounding the steel-liner. Besides these rather rudimentary hydraulic based monitoring systems, a number of more sophisticated techniques for pipeline leak detection involving transient pressure waves have been applied in water, gas and oil networks [Misiunas *et al*, 2005[6]; Stephens *et al.*, 2008[7]; Taghvaei *et al.*, 2010[8]]. Therefore, a new monitoring method for steel-lined pressure shafts and tunnels based on the Fluid-Structure Interaction and on the processing of the wave reflections during water hammer has been developed and is presented herein. It is a real time procedure that can detect the occurrence, severity and location of a change of wall stiffness of shafts and tunnels based on recorded dynamic pressure signals at their both accessible ends.

3 PHYSICAL SCALED MODEL

3.1 DESCRIPTION OF THE EXPERIMENTAL SET-UP

If the hypothesis of an axi-symmetrical deformation of the multilayer system (steel–concrete–rock) of the pressure shaft is accepted, the shaft can be modeled by a one layer system. The experimental facility shown in Fig. 1 was built at the Laboratory of Hydraulic Machines (LMH) of the Ecole Polytechnique Fédérale de Lausanne (EPFL). Water hammer events can be generated inside the multi-reach test pipe by closing a shut-off valve at its downstream end. The test pipe has an internal diameter of 150 mm and a length of 6.25 m measured from the shut-off valve to the upstream air vessel. It is supplied with water from a reservoir through a variable speed pump and a 10 m supply PVC conduit. The test pipe is divided into several reaches of 0.5 m and 1.0 m length fitted together with flanges having an external diameter of 285 mm and a thickness of 24 mm. The flanges are also used to rigidly fix the test pipe along its length in order to minimize any longitudinal and transversal movements during the tests. An electromagnetic flow meter is placed on the supply conduit to measure the steady state flow inside the facility. On the highest point of this conduit, an air purge valve is installed to evacuate the captured air inside the test rig. A first control and security valve followed by an elastic deformable joint are located at the downstream end of the supply conduit, which is protected against water-hammer by the pressurized air vessel. The shut-off valve is operated automatically by an air jack with an input and output electro-valves. The volume of air needed to activate the jack is provided by an air compressor with a constant pressure of 10 bars. The shut-off valve is followed by a purge valve, two elbows, an elastic joint and a second control valve located at the entrance of the supply reservoir. The total length of the test pipe comprising all these pieces is about 2 m. The opened and closed states of the shut-off valve are detected by two infrared diffuse sensors. The data acquisition system includes: (i) two pressure transducers (HKM-375M-7-BAR-A, Kulite) with a pressure range from 0 to 7 bars and an accuracy of 0.5%, (ii) a NI-USB-6259 acquisition card M series with 32 analogue input channels and 2 analogue output channels to activate the two electro-valves of the shut-off valve, and (iii) a notebook computer connected to the acquisition card through a USB cable. The sampling frequency was fixed to 15 KHz. LabView 8.6, MATLAB 2008b and Diadem 11.0 software were used for acquiring, controlling and processing the experimental data.

The different test pipe configurations are shown schematically in Figure 2. All tests were carried out with an initial steady flow of 58 l/s and an initial mean water pressure of 0.2 bar measured at the sensor position P2.

3.2 TESTS RESULTS AND ANALYSIS

An example of the measured pressure records at P1 and P2 is shown in Figure 3 for three test pipe configurations. The water hammer wave speed is the ratio of the distance separating the pressure sensors (equal to 5.88 m) and the wave travel time between them. In case of steep wave fronts, the travel time is the one that separates the time at the maximum values of these fronts. The mean and standard deviation of the computed wave speeds for 84 tests carried out on the seven test pipe configurations are shown in Figure 4. A significant decrease of the wave speed is observed in “Steel+PVC” configurations. It is an indicator of the presence of weak reaches in the pipe or in the shafts of hydropower plants. This decrease of the wave speed is not very well marked in case of “Steel+Alu” configurations. In the case of water hammer pulses induced by the progressive stoppage of flow by the shut-off valve, no clear pressure wave front can be identified. Therefore, another approach is used to estimate the wave speed between the two pressure sensors [Hachem and Schleiss, 2011[10]].

To locate the weak reach inside the test pipe or inside the shaft, the wave reflections and transmissions are processed. As it is shown in Figure 5, an incident pressure wave is divided into transmitted and reflected waves when crossing the weak reach [Wylie *et al.*, 1993[9]]. Figure 6 gives the theoretical values of the ratio between water hammer transmission and reflection in function of the ratio between elasticity modulus of the weak reach and the other parts of the test pipe. PVC reaches having an E_{PVC}/E_{steel} equal to 0.014, generate reflections up to 38% of the incident wave. In case of Aluminum reaches, these reflections are around 1%. This low ratio induces difficulties in detecting and capturing the reflection pressure signals in presence of noise. In low dissipative media, a weak reach with an elasticity modulus not higher than 10% relative to the other part of the structure could be located by processing the pressure reflection data. The analysis of pressure records to locate the weak reach is performed using the Fast Fourier Transform and the Wavelets techniques [Hachem and Schleiss, 2011[11]].

4 PROTOTYPE MEASUREMENTS

4.1 DESCRIPTION OF THE SITE

The Grimsel II pumped-storage power plant is situated in the Canton of Bern in the heart of Switzerland at an altitude of 1760 m.a.s.l (see Figure 7) and under operation since 1982. It is owned by *Kraftwerke Oberhasli AG* (KWO[12]) and has an underground power house with four reversible pump-turbine Francis groups of a total capacity of 350 MW. A headrace tunnel of 4 km length and 6.8 m of internal diameter relates the Oberaar Lake (the upper reservoir) to the vertical surge tank of 16 m of diameter and 123 m height. This surge tank is followed by the security butterfly valve and by a steel-lined shaft of 3.8 m of internal diameter and 650 m length. The upstream end of the shaft is connected to an inclined tunnel of 170 m length which is the extension of the shaft excavation. It functions as an inclined surge tank. The steel-lined shaft has a slope of 100% and conveys water from elevation 2213 m.a.s.l. to the power house. At the low pressure side downstream from the pump/turbine groups, a third vertical surge tank of 8 m of diameter and 155 m height is connected laterally to the tailrace steel-lined tunnel of 300 m length connecting the power house to Grimsel Lake (the lower reservoir). Figure 8 shows a schematic 3d view of this water conveying system including the shaft, the surge tanks and the power house. The two positions of the pressure sensors P1 and P2 and the lateral cross-section of the steel-lined shaft are also shown.

4.2 IN-SITU MEASUREMENTS

The two data acquisition systems at P1 and P2 are actually in the test phase. Each system contains one high resolution pressure sensor, an acquisition card and a PC. They are synchronized via a fiber optic connection and they can be accessed on-line from the LCH laboratory (Laboratoire de Constructions Hydrauliques) in Lausanne.

The first preliminary data are very promising and the ongoing work will consolidate the stability of the two acquisition systems. The wave speed estimation procedure will be validated during start-up and shut-down of pumps and turbines with a special focus on wave dissipation and dispersion intensities. The localization procedure of weak reaches will be implemented with the purpose to detect the location of some eventual geological and geotechnical weak zones of the rock mass surrounding the steel liner. The estimated locations will be compared with the real ones which can be obtained from the existing as-built drawings of the shaft.

5 CONCLUSION

A new monitoring procedure for detecting the local drop of wall stiffness of steel-lined pressure tunnels and shafts is outlined in this paper. It uses the water hammer pressure records to identify the presence of the weak reach and to extract its location and severity. This monitoring method is based on the theoretical approach of water wave reflections induced by the pressurized water reaches with different hydro-acoustic parameters. It has been validated by a series of experimental tests that have been carried out on a physical scaled facility. The assessment of in-situ pressure data that are measured at the shaft of a pumped-storage power plant are now in process to test and extend the monitoring method to real scale structures.

Acknowledgments

The study is part of the research project *HydroNet* (Modern methodologies for the design, manufacturing and operation of pumped storage plants) funded by the *Swiss Competence Center Energy and Mobility* (CCEM-CH), the *swisselectric research* and the *Swiss Office for Energy*. *Kraftwerke Oberhasli AG* (KWO) supported the installation and the operation of prototype measurements.

References

1. Schleiss, A.J., “The importance of hydraulic schemes for sustainable development in the 21st Century”, *The International Journal of Hydropower & Dam*, Vol. 7, Issue 3, 2000

2. Competence Center Energy and Mobility (CCEM), www.ccem.ch

3. Swisselectric research, www.swisselectric-research.ch

4. Hachem, F.E. and Schleiss, A.J., “The design of steel-lined pressure tunnels and shafts”, *The International Journal on Hydropower & Dams*, Vol. 16, Issue 3, 2009

5. Hachem, F.E. and Schleiss, A.J., “A review of wave celerity in frictionless and axisymmetrical steel-lined *pressure* tunnels”, *Journal of Fluids and Structures*, 27, 2011

6. Misiunas, D., Vitkovsky, J., Olsson, G., Simpson, A., and Lambert, M., “Pipeline break detection using pressure transient monitoring”, *Journal of Water Resources Planning and Management*, 131(4), 2005

7. Stephens, M.L., Simpson, A.R., and Lambert, M.F., “Internal wall condition assessment for water pipelines using inverse transient analysis”. *Proceedings of the 10th Annual Symposium on Water Distribution Systems Analysis*, ASCE, Kruger National Park, South Africa, 2008

8. Taghvaei, M., Beck, S.B.M., and Boxall, J.B., “Leak detection in pipes using induced water hammer pulses and cepstrum analysis”, *International Journal of COMADEM*, 13(1), 2010

9. Wylie, E.B., Suo, L., and Streeter, V.L., “Fluid Transients in Systems”, facsimile edition, Prentice Hall, Englewood Cliffs, NJ, 1993

10. Hachem, F.E. and Schleiss, A.J., “Physical tests for estimating the water-hammer wave speed in pipes and tunnels with local weak wall stiffness”, *Proceedings of 2011 World Environmental & Water Resources Congress (EWRI)*, Palm Springs, California, May 2011

11. Hachem, F.E. and Schleiss, A.J., “Detection of local wall stiffness drop in steel-lined pressure tunnels and shafts of hydroelectric power plants using steep pressure wave excitation and wavelet decomposition”, *Journal of Hydraulic Engineering*, under review (second round), 2011

12. KWO, Kraftwerke Oberhasli AG, Innertkirchen, Switzerland, www.grimselstrom.ch

List of Figures

Appendix for Figures and Tables

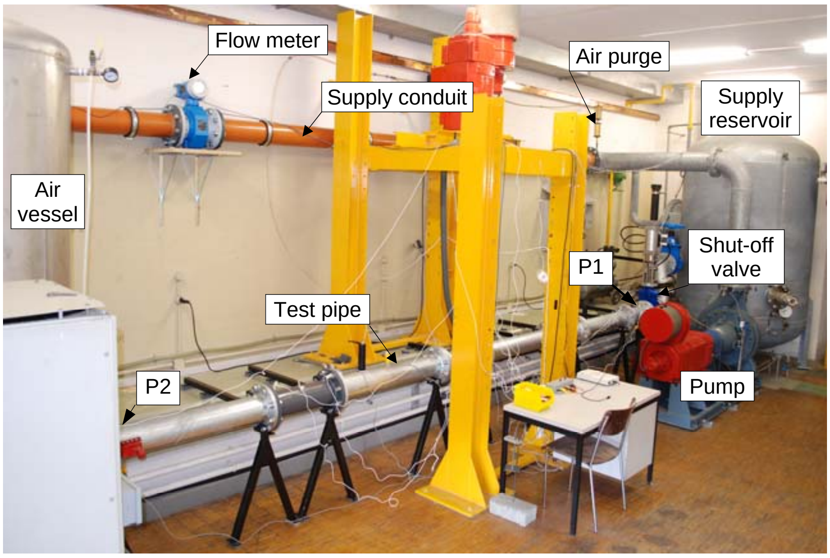

Figure 1.

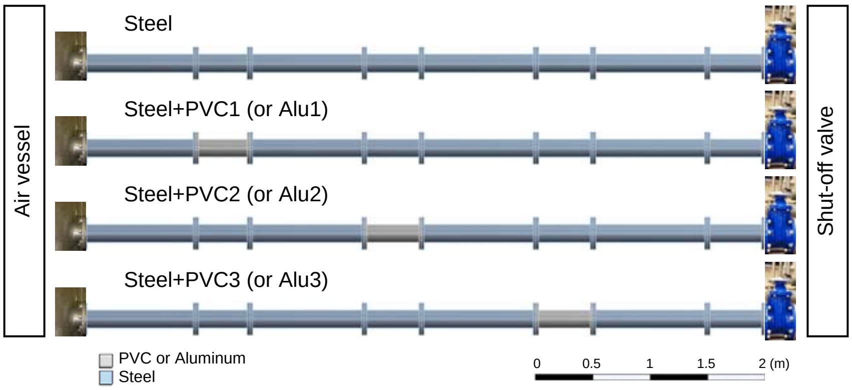

Figure 2.

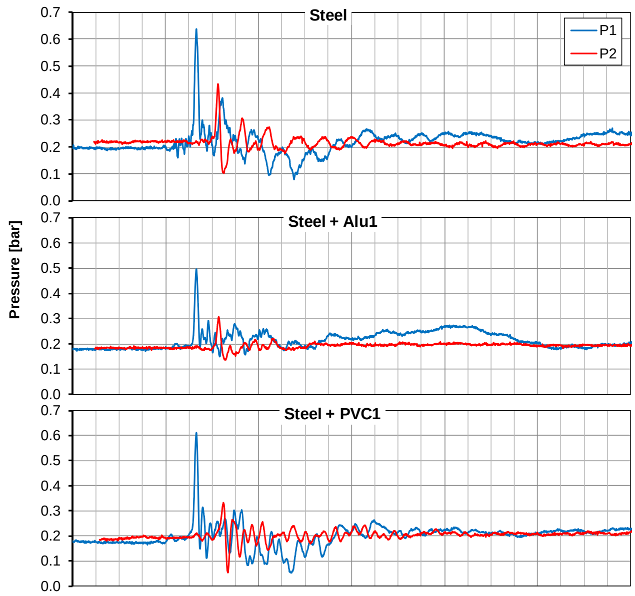

Figure 3.

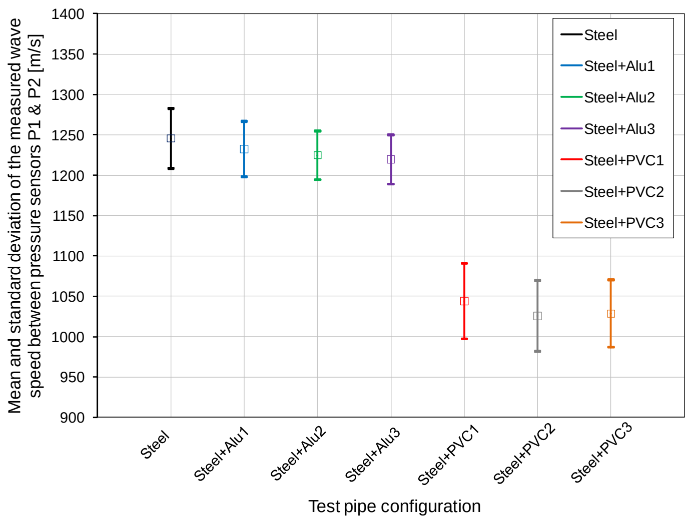

Figure 4.

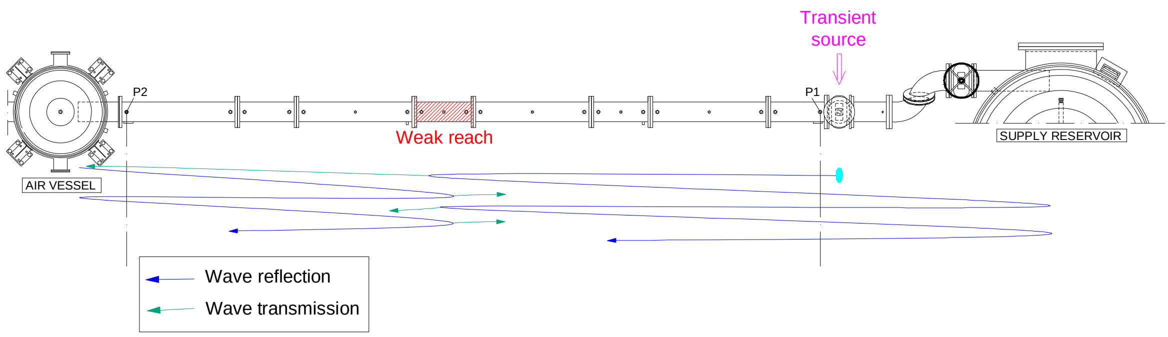

Figure 5.

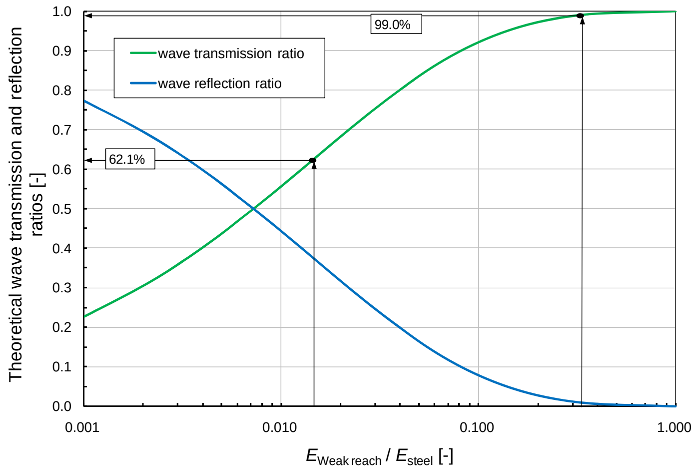

Figure 6.

Figure 7.

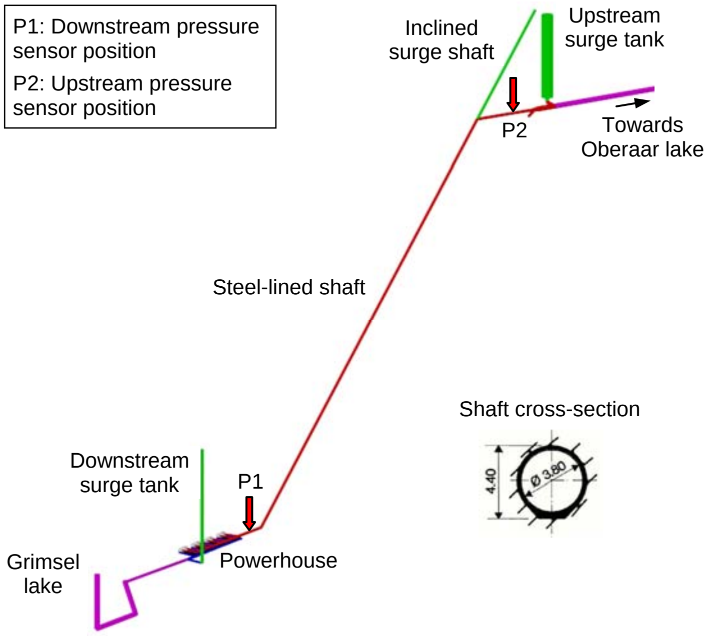
P1: Downstream pressure sensor position
P2: Upstream pressure sensor position
Inclined surge shaft
Upstream surge tank
P2
Towards Oberaar lake
Steel-lined shaft
Shaft cross-section
4.40
Ø 3.80
Downstream surge tank
P1
Powerhouse
Grimsel lake

Figure 8

On-line monitoring of steel-lined pressure shafts by using pressure transient signals under normal operation conditions

F.E. Hachem, M.ASCE[1] and A.J. Schleiss[2]

[1]Researcher-assistant, Laboratory of Hydraulic Constructions (LCH), Ecole Polytechnique Fédérale de Lausanne (EPFL), Station 18, 1015 Lausanne, Switzerland.
fadi.hachem@a3.epfl.ch
[2]Professor and Director, Laboratory of Hydraulic Constructions (LCH), Ecole Polytechnique Fédérale de Lausanne (EPFL), Station 18, 1015 Lausanne, Switzerland.
anton.schleiss@epfl.ch

Abstract
The local deterioration of the mechanical properties of steel-lined pressure shafts and tunnels induces a decrease of the celerity and an increase of the energy attenuation of water-hammer wave. This deterioration may arise from the weakening of the backfill concrete and the surrounding rock mass which provide the radial support of the steel liner. A new on-line monitoring system implemented and tested at the Grimsel II pumped-storage shaft in Switzerland is presented. The difficulties encountered during the in-situ measurements are outlined. The new monitoring approach is based on acquiring and analyzing the dynamic pressure data generated by the normal operation of pumps and turbines. The wave celerity and the exponential attenuation coefficient of water-hammer wave are estimated based on pressure records. Monitoring charts for these indicators are established using the statistical quality control method. The results show a stable monitoring scheme that needs longer acquisition data series to consolidate its control limits.

Keywords: Water-hammer; Wave celerity; Wave attenuation; Steel-lined pressure shafts and tunnels; Monitoring, Statistical quality control.

Introduction

The structural weakening of the backfill concrete and rock mass surrounding the steel-liner of pressure shafts and tunnels modifies the load distribution ratio between the three components steel, concrete and rock of the wall system. Thus, the stresses in the steel liner may generate yielding in the case of traditional steel or crack initiation and propagation for high-strength steel. In the worst case, brittle failure of the steel liner can occur which may produce catastrophic landslides due to hydraulic jacking of the surrounding rock mass and important economic losses.

A drop of radial stiffness of pipelines and steel-lined shafts and tunnels induces also a drop of wave speed values and an increase of the wave attenuation due to the transmission/reflection phenomenon (Wylie *et al.*, 1993; Hachem and Schleiss, 2011c). A transient based assessment method for detecting the formation of weak reaches by monitoring the celerity and the attenuation of the wave is presented in this paper. These indicators are estimated using the water-hammer pressure data acquired continuously in the pressure shaft of a pumped-storage power plant. The pressures are generated by normal closing and opening operations of pumps and turbines at the powerhouse. This assessment method can be considered as the first alarm indicator of a complete monitoring procedure. If the formation of weak reaches is detected somewhere along the pressure shaft, a second monitoring step is launched for leak detection. The latter is possible through many available techniques that have been applied in water, gas and oil networks (Beck *et al.*, 2005; Covas et al, 2005; Hunaidi, 2006). If a leak is detected, the last step of the monitoring process starts with the emptying of the conveying system followed by visual inspections, non-destructive investigations and repairs.

Theoretical background

Water-hammer wave speed and wave attenuation

A change in celerity and energy attenuation of water-hammer wave is induced by the local change of the mechanical properties of the tunnel or shaft wall. This behavior can be explained by using a Fluid-Structure Interaction (FSI) model in which the effect of the backfill concrete and the surrounding rock mass is mechanically modeled by a Kelvin system including a spring (with a radial stiffness coefficient, Ks_r), a dashpot (with a radial damping coefficient, C_r), and an additional mass (M_r) (Hachem and Schleiss, 2011a). Therefore, the mechanical properties of the shaft wall can be expressed by one coefficient, K_r, as follows:

$$K_r = r_i^2 \left(Ks_r + \mathrm{i}\omega C_r - \omega^2 \left(M_r + \rho_s e \right) \right) \tag{1}$$

where, r_i is the internal radius of the steel liner, ω is the angular frequency (=2πf) of the excitation of frequency f, ρ_s and e are the unit mass and thickness of the steel liner, respectively, and i is the complex number $(-1)^{0.5}$. In such model, the wave speed c_0 is given by the formula:

$$c_0 = \sqrt{\frac{1}{\rho_w \left(\frac{1}{K_w} + C \cdot \frac{2 r_i}{E_s\, e} \right)}} \tag{2}$$

in which,

$$C = \frac{1 - \nu_s^2}{1 + (1 - \nu_s^2) K_r / E_s\, e} \tag{3}$$

and where, E_s is the elasticity modulus of steel, ν_s is its Poisson's ratio, and ρ_w and K_w are the unit mass and the bulk modulus of water, respectively.

The solution, k (which is the ratio of the wave speed c_0 to the complex wave speed c) of the quadratic dispersion equation of the FSI model for the water-hammer propagation mode yields to the following pressure expression:

$$p_i = \hat{p}_i \cdot \mathrm{e}^{-\phi y/\lambda} \cdot \mathrm{e}^{\mathrm{i}\omega (t - y/c)} \tag{4}$$

where, φ is the logarithmic decrement of the wave ($= -2\pi \mathrm{Im}(k/c_0)/\mathrm{Re}(k/c_0)$) in which Im( ) and Re( ) are the imaginary and real parts of the complex number k/c_0, $\hat{p}_i$ is the reference water pressure inside the shaft, y is the longitudinal coordinates along the shaft axis, t is the time, and λ is the wave length of the water-hammer mode (=c_0/f). The logarithmic decrement φ is called the wave attenuation coefficient throughout this paper.

Statistical quality control method

The statistical quality or process control is a procedure that sets control limits on the normal operating condition of the system based on initial assessments of the mean and standard deviation of features or characteristics derived from the system data. The control or monitoring chart is a graphical display of the feature that has been measured or computed from a data sample versus the sample number or time. It contains a center line (CL) that represents the average value of the feature corresponding to the in-control state and two other horizontal lines, called the upper control limit (UCL) and the lower control limit (LCL). These control limits are chosen in a way that the process will be considered in control if nearly all the sample points fall between them.

For variables such as the wave speed and the wave attenuation coefficient, both the mean of the estimated values and their variability are used. The control of the process average or mean quality level is done with the so-called $\bar{x}$ chart while the process variability is monitored with a control chart for the range, called R chart. For m samples available each containing n observations x_i on the quality characteristic (m subgroups of n samples), the CL, LCL and UCL of the general control model, known as Shewhart model, are given as follows (Montgomery, 2005):

$$\bar{x}\text{ chart, }\begin{cases}\mathrm{UCL}=\dfrac{\sum_{j=1}^{m}\overline{x_j}}{m}+\mathrm{Lim}\cdot\dfrac{1}{\sqrt{n}}\cdot\dfrac{1}{f_{\mathrm{Mean}}}\dfrac{\sum_{j=1}^{m}R_j}{m}\\ \mathrm{CL}=\dfrac{\sum_{j=1}^{m}\overline{x_j}}{m}\\ \mathrm{LCL}=\dfrac{\sum_{j=1}^{m}\overline{x_j}}{m}\text{-}\mathrm{Lim}\cdot\dfrac{1}{\sqrt{n}}\cdot\dfrac{1}{f_{\mathrm{Mean}}}\dfrac{\sum_{j=1}^{m}R_j}{m}\end{cases}\qquad R\text{ chart, }\begin{cases}\mathrm{UCL}=\dfrac{\sum_{j=1}^{m}R_j}{m}+\mathrm{Lim}\cdot\dfrac{f_{\mathrm{Std}}}{f_{\mathrm{Mean}}}\cdot\dfrac{\sum_{j=1}^{m}R_j}{m}\\ \mathrm{CL}=\dfrac{\sum_{j=1}^{m}R_j}{m}\\ \mathrm{LCL}=\dfrac{\sum_{j=1}^{m}R_j}{m}\text{-}\mathrm{Lim}\cdot\dfrac{f_{\mathrm{Std}}}{f_{\mathrm{Mean}}}\cdot\dfrac{\sum_{j=1}^{m}R_j}{m}\end{cases}\qquad(5)$$

where, $\overline{x_j}$ is the mean value of x_i in each n observations, f_{Mean} and f_{Std} are the mean and the standard deviation of the relative range variable $RR=R/\mathrm{Std}_{\mathrm{pop}}=(x_{\max}-x_{\min})/\mathrm{Std}_{\mathrm{pop}}$, respectively, $\mathrm{Std}_{\mathrm{pop}}$ is the standard deviation of the population x, and Lim is the distance of the control limits from the CL, expressed in standard deviation units. The Lim value is generally taken equal to 3 according to the “Three-sigma” criterion.

It should be noted here that the above development assumes that the variable x is normally distributed. Burr (1967) has noted that the control limits are very robust to the normality assumption and can be employed unless the population is extremely non-normal. The work of Yourstone and Zimmer (1992) showed that, in most cases, samples of size higher than n=4 are sufficient to ensure reasonable robustness to the normality assumption. This value of n is also suitable to detect moderate to large process shifts. For n=4, the mean and the standard deviation of the relative range variable RR are 2.059 and 0.88, respectively. For n=6, these values are 2.534 and 0.848, respectively (Montgomery, 2005).

The implementation and use of the monitoring charts follow two phases. In the first phase, the control limits are set based on a number of subgroups m, generally higher than 20. The observations inside these subgroups represent the present or basic state of the monitored variable. The control limits established in this phase are used in the second phase for future on-line monitoring of the variable values.

Prototype measurements

Description of the site

The pressure shaft of the Grimsel II pumped-storage plant has been equipped with two high sensitive pressure sensors. The plant is owned by Kraftwerke Oberhasli AG (KWO) and is located in the Canton of Bern, in the central part of Switzerland. It has an underground powerhouse equipped with four pump and turbine groups. A 4 km long headrace tunnel connects the Lake Oberaar (the upper reservoir) to the vertical surge tank. A security butterfly valve is installed downstream of the surge tank and followed by the steel-lined shaft which has a slope of 100% (45^{o}), an internal diameter of 3.8 m, and a length of about 760 m. The upstream end of the shaft is connected to a 170 m long inclined tunnel which is an extension of the pressure shaft excavation and functions together with the main surge tank as an inclined surge shaft. An accessible steel-liner reach of about 1.5 m is located just upstream of the bifurcation which distributes the water at the high pressure side to the four machines inside the powerhouse. Fig. 1 shows in detail a 3D view of the high pressure side of the waterway of Grimsel II pumped-storage plant with some important point coordinates and paths lengths. The locations of the measurement stations S1 and S2 and the typical lateral cross-section of the steel-lined shaft are also shown.

Instrumentation and data acquisition system

Two dynamic piezoresistive pressure sensors of type “Kistler 4045A” with an absolute pressure range of 100 bars for P1 (at Station S1) and 20 bars for P2 (at Station S2) have been used. The constant DC electrical excitation current of 24 V needed for these sensors, is provided after transformation of the 48 VDC current available in the powerhouse and in the security valve cavern. The output signals of the pressure sensors are amplified by a “Kistler 4618A2” amplifier type. The pressure sensor P1 is screwed inside a hole made in the elbow of the shaft drainage conduit of 150 mm in diameter while sensor P2 is fixed on the cover plate of the shaft drainage reach of 200 mm in diameter. Each data acquisition station contains one pressure sensor, one “NI-USB-6259 M series” acquisition card and one industrial PC. The existing output current of the Venturi measurement system has been used to extract the total flow discharge of pumps and turbines. The control commands of the spherical valves in the powerhouse are sent from the KWO control center and are transformed by an electric relay to a trigger signal of 0-10-0 VDC with a plateau of 3 s. The Venturi and trigger output signals have been connected to the measurement system at S1.

The data acquisition software is based on LabVIEW programming platform. The data are acquired continuously in time at a sample frequency of 1 kHz and they are stored once the trigger signal rises from 0 to 10 V. The total storage time has been fixed to 600 s and includes the steady-state and the transient parts of the pressure signals. The storage loop starts by opening a data file of format TDMS and assigning the date given by the PC clock to the storage directory name. It ends automatically after the end of the storage duration fixed by the user.

The synchronization of the two acquisition systems is done via a fiber optic cable which connects the two stations PCs to the KWO server inside the powerhouse. Every one hour, the internal clocks of the two PCs are automatically synchronized with the server time. The trigger signal acquired at S1 is saved by the acquisition software as a shared variable type and sent to the PC of station S2. This type of network-published variables can be used to write and read across an Ethernet network. The two measurement stations can be controlled via a Virtual Private Networking (VPN) connection. The acquired data can be accessed on-line by this secured internet connection.

Dynamic pressure obtained from normal operation conditions

During start-up of pumps and turbines

In Grimsel II pumped-storage plant, the pump start-up is preceded by a start-up and shut-down of the turbine of another Francis unit. This produces the electrical power needed to launch the pump motor. The beginning of the turbine shut-down maneuver generates a steep positive increase of pressure at P1 of about 1.8 bars in amplitude and 1.5 s in duration. After 12 s from the beginning of the turbine shut-down, the outlet valve of the pump is opened and the total flow increases and reaches -20 m^3/s in about 50 s (negative discharge indicates pumping flow). After the end of the start-up maneuvers, the mass oscillation between the upper reservoir and the surge system generates pressure fluctuations inside the system. Being not relevant for the monitoring of the pressure shaft, these fluctuations are ignored. The start-up of the pump motor coupled with the fluid-structure interaction between the water and the liner generates high frequency pressure fluctuations of around 100 Hz. These pressures are detected at both pressure sensors.

During the turbine start-up, the valve at the bypass conduit of the spherical valve is first opened to balance the water pressure between its both sides. The inlet valve is then gradually opened simultaneously with the wicket gates. Pressure fluctuations having maximum amplitude around 1 bar and a frequency near 0.46 Hz are generated by the opening of the pressure balance bypass. At measurement station S2, the pressure fluctuations induced by the bypass opening have small amplitude. The main part of energy of the water-hammer waves are reflected back to the powerhouse by the junction at point 2 (Fig. 1).

It can be concluded that the most relevant parts of the pressure measurements in both start-up of pumps and turbines are those acquired during the opening of the spherical valve. They contain the water-hammer fluctuations which are generated directly after the steady-state condition. This allows following the first wave front between sensors P1 and P2 to estimate the value of the water-hammer wave speed. These parts of the pressure signals of 130,000 samples in length are shown in Figs. 2 and 3 for the start-up of pumps and turbines, respectively.

During shut-down of pumps and turbines

During the normal pump shut-down, the spherical valve is first closed slowly and then the power supply of the pump motor is switched off. The closure time of the spherical valve during the pump shut-down is about 70 s. The total flow discharge decreases from -20 m^3/s to zero. At the beginning of the valve closing maneuver, an important drop of pressure at P1 of about 6.5 bars is observed. It propagates upstream towards the surge system and is detected by P2 sensor. The front steepness of this pressure drop is around 4.5 s. Pressure fluctuations of 2 bars in amplitude and 0.46 Hz in frequency are observed at around 22 s after the time of the minimum pressure peak at P1.

The normal turbine shut-down mode begins with the electric load rejection of the generator followed by the simultaneous closure of the wicket gates and the spherical valve. A small increase of pressure at P1 of about 0.3 bar is detected at the beginning of the maneuver. It is followed by pressure fluctuations having a maximum amplitude of 0.5 bar and then by more important perturbations of around 0.8 bar in amplitude near the end of the maneuver. The latter perturbations are detected by the pressure sensor P2.

The most relevant parts of the pressure signals which are analyzed herein are shown in Figs. 4 and 5 (selected inside a time window of 130,000 samples) for the shut-down of pumps and turbines, respectively.

Data analysis

Assessment of water-hammer wave speed

Using the signals of the two pressure sensors P1 and P2

Different time-based techniques have been used to estimate the travel time between the pressure sensors P1 and P2. The pressure records were first filtered by using Daubechies (db10) mother wavelet and the summation of the decomposition details from D8 to D12 has been considered (Mallat, 1990; Ferrante and Brunone, 2003; Hachem and Schleiss, 2011b). For the start-up of pumps and turbines, the approach based on the time separating the intersection points of two regression lines correlating the steady-state and the first front pressure of each of them is used. During shut-down of pumps, P1 pressure record was first differentiated relative to time and then cut, with the pressure P2, inside a window time having the lower border at the beginning of the sampling and the upper one at the first maximum peak of P2. The procedure ends by cross-correlating the two signals in order to determine the travel time between them. Finally, for the turbines shut-down case, two approaches were used. The first approach extracts the time that separates the maximum values of the front pressure measurements while the second uses the same approach as for the pumps and turbines start-up. The mean value of the two estimated travel times is retained.

The wave speed values estimated from the time lag between the first wave front of pressures P1 and P2 show scattered patterns. This is specially observed during pumps and turbines start-up and turbines shut-down modes. The estimation method was affected by the following sources of error: (i) the unknown synchronization time delay of the internal clocks of the PCs of the two acquisition systems, (ii) the alteration and dispersion of the pressure signals, and (iii) the accuracy of the assessment methods.

Regarding the first point, and in spite of the fact that important effort has been made to build the synchronization scheme, the results show that the method adopted was not reliable. In fact, the server used to synchronize the internal clock of the PCs is located inside the powerhouse. Therefore, the time needed by the two acquisition systems to access the server is not exactly the same. For example, an accuracy in the order of 100 ms induces an error of around 20% on the wave speed between the two sensors. Another method of synchronization which does not use the internal clock of the PCs, consists on sending an electrical current pulse at the moment of trigger from the powerhouse towards the upstream measurement station. This method is more accurate than the one that has been used. Unfortunately, its application to the Grimsel II plant was not possible because of the absence of an electrical cable connecting the two stations.

The second source of error is related to the alteration, dissipation and dispersion of the water-hammer wave when it crosses the junction between the headrace pressure tunnel and the inclined surge shaft (point 2 on Fig. 1). At this junction, the major part of the wave energy (above 75%) is reflected back to the powerhouse. The special waterway layout of the Grimsel II plant with an inclined surge shaft located between the two measurement stations has significantly reduced the efficiency of the applied methods used to estimate the wave speed values.

Finally, the accuracy of the assessment methods is closely related to noise level which affects the measurement records. The mean signal to noise ratio at station S1 was around 1,241. The reflection of the water-hammer wave at the surge shaft junction has reduced this ratio to 169 for the measurements at station S2. The decrease of the signal to noise ratio induces higher error in the computed travel time of the wave between the pressure sensors and reduces the accuracy of the determination of the wave speed.

Using Fast Fourier Transform (FFT) of pressure record P1

In this approach, the water-hammer wave speed inside the pressure shaft is obtained by the FFT applied to the pressure record P1. The FFT with Hanning windowing has been used and the normalized RMS density spectrums of the 396 acquired files during pumping and generating modes have been computed. The normalization is obtained by dividing all the FFT magnitudes by their maximum valued computed inside the frequency interval of interest [f_{min}, f_{max}]. These frequencies are determined according to the following equations:

$$f_{min} = a_{min}/4L_{max} = 0.21\,\text{Hz} \tag{6}$$

$$f_{max} = a_{max}/4L_{min} = 35\,\text{Hz} \tag{7}$$

in which a_{min} and a_{max} are the two logical wave speed values of 800 m/s and 1,400 m/s, respectively, $L_{max} \approx 975$ m is the path length between points 1 and 4 of Fig. 1, and $L_{min} \approx 10$ m is the path length 1-a shown on the same figure. The FFT density spectrum of the pressure signal P1 depicted in Fig. 3(a) is shown in Fig. 6. This spectrum shows clearly a strong peak near frequency 0.46 Hz with weaker peaks at higher frequencies. The 0.46 Hz is the fundamental frequency, f_{fund}, of the shaft. It corresponds to the water-hammer propagation between the downstream end of the distributor and the main reflection border located at the junction between the pressure and the surge shafts (points 1 and 2 on Fig. 1, respectively). Similar FFT results have been observed for the other pumping and generating modes. Once the fundamental frequency is obtained, the wave speed can be estimated from the following formula:

$$a = 4\,L_{1-2}\,f_{fund} \tag{8}$$

where, L_{1-2} is the shaft length between points 1 and 2. For L_{1-2} equal to 762.34 m, the estimated wave speed is 1,402.7±23.5 m/s for a minimum FFT resolution of ±0.0077 Hz. The wave speed values estimated by the FFT approach the 396 files acquired between February 17 and June 10, 2011 have a mean and standard deviation values of 1,433.3 m/s and 35.7 m/s, respectively. The mean of the estimated wave speed is 5.3% higher than the theoretical value of 1,361.5 m/s calculated using the quasi-static formula for the steel-lined pressure shafts surrounded by cracked backfill concrete and rock mass (Hachem and Schleiss, 2011a) and the parameters values given in Pahl *et al.* (1989). The discrepancy between the values of the estimated and theoretical wave speed can be explained by the uncertainties in the length of the pressure shaft and the frequency or the wave travel time between points 1 and 2 shown in Fig. 1. The application of the error propagation approach (Coleman and Steele, 1999) to Eq. 8 with a bias error in f_{fund} equal to 0.0077 Hz and an error of 10% in the pressure shaft length yields to an uncertainty in the wave speed of ±140 m/s.

A more detail analysis of the FFT spectrums reveals also that some peaks are nothing else than the odd harmonics of the fundamental frequency while others can be related to certain known features of the shaft. For example, Fig. 6 reveals an interesting peak at 2.46 Hz. The shaft length associated to this frequency (Eq. 8) is equal to 142.6 m. This value is close to the pressure shaft length between points 1 and 8 (Fig. 1). At point 8, a significant increase of the stiffness of the shaft wall is present. The thick backfill concrete layer and the elbow of the shaft at this point create wave reflection boundaries for the pressure waves.

The problems encountered during the application of the methods based on processing the data of the two pressure sensors P1 and P2 have made these methods inapplicable in case of the Grimsel II power plant. Therefore, the wave speed values estimated from the FFT approach have been used to establish the monitoring charts for the water-hammer wave speed.

Estimation of the wave attenuation coefficient

The special scheme of the monitored pressure shaft in which a surge inclined shaft is located between the two measurement stations, induces important attenuation of the water-hammer wave between sensors P1 and P2. This high attenuation combined with low signal-to-noise ratio at pressure sensor P2 can hide small increase of the wave attenuation indicator which can be induced by the formation of weak reaches along the pressure shaft. Therefore, the wave attenuation coefficient φ of the pressure record P1 has been only used for establishing the monitoring charts.

The estimation of φ have been done after rearrangement of Eq. 4 in which, $\hat{p}_i = \max(\mathrm{P1})$, $y = s \cdot a/f_{\mathrm{fund}}$, $\lambda = a/f_{\mathrm{fund}}$, $\omega = 2\pi f_{\mathrm{fund}}$, and $s = t/T_{\mathrm{fund}}$ is the dimensionless number of the fundamental period of water-hammer wave inside the Grimsel II pressure shaft. This yields to the following equation:

$$\mathrm{P1} = \max\left(\mathrm{P1}\right) \cdot \mathrm{e}^{-\phi \cdot s} \tag{9}$$

The values of φ have been then obtained by fitting an exponential regression curve on the normalized Root Mean Square, $\mathrm{Norm(P1)} = \mathrm{RMS(P1)} / \max\left[\mathrm{RMS(P1)}\right]$, of the filtered pressure signal P1. The pressure records are filtered by using Daubechies (db10) mother wavelet where only details from D8 to D12 have been retained. The resolution of the RMS is taken equal to 1,000 Hz / 0.46 Hz ≈ 2,175.

Fig. 7 shows the normalized RMS points and the exponential regression equations of the pressure record P1 given in Fig. 3(a). A very good agreement is found between the RMS values of the filtered pressure measurements and the exponential law given in Eq. 9. A similar behavior has been observed for all the pressure P1 acquired during the pumping and generating modes.

The computed values of φ obtained from the 396 acquired data files are shown in Fig. 8 for pumping and generating modes. For the pump and turbine start-up modes, Fig. 8(a) shows scattered pattern of φ with values ranging between 0.14 and 0.05. The R^2 value of the regression law are higher than 0.8. In the turbine shut-down mode, the φ values are plotted in a very compacted pattern. They show a positive shift of about 0.01 from May 05, 2011 onward (Fig. 8(c)). Additional measurements are needed in order to explain this increase of the attenuation coefficient. The corresponding R^2 values are excellent (higher than 0.976). During the pump shut-down maneuvers, the wave attenuation coefficient histories show similar behavior as in the turbine shut-down mode with more scattering values (Fig. 8(b)). The R^2 values of this mode are close to the pump and turbine start-up case.

The results reveal the existence of two different families of φ with a mean of 0.078 and a standard deviation of 0.015 for the pump and turbine start-up modes and a mean and standard deviation of 0.035 and 0.015, respectively, for the shut-down modes. The relative difference between the φ means is about 55%. The higher wave attenuation detected in pump and turbine start-up modes can be explained due to the additional wave attenuation resulting from the opened bypass of the spherical valve inside the powerhouse. This boundary condition of the pressure shaft can also explain the scattering of the attenuation coefficient values shown on Fig. 8(a).

Development of monitoring charts

Monitoring charts for water-hammer wave speed

Figs. 9(a) and 9(b) show the $\bar{x}$ and R monitoring charts, respectively, of the wave speed inside the pressure shaft of the Grimsel II plant. The control limits have been defined by classifying 396 subsequent records in 66 subgroups (m=66) of 6 samples each (n=6). All the points fall inside or near the control limits of $\bar{x}$ chart and no systematic pattern behavior is detected. Also, the points plotted on the R chart do not show a specific pattern behavior but they have four points, between April 27 and May 22, that fall relatively far above the UCL limit. These points are generated by some unusually high values of the estimated wave speed. All these high

values are computed from pressures acquired during the start-up modes of pumps and turbines. It is clear that the control limits of the monitoring charts can be revised by discarding the points that are out-of-control and by using only the remaining in-process points. Such adjustment will be more relevant if it is done after acquiring a longer series of in-situ measurements.
Dealing with the available data, the observations indicate that the process is in control in the present time and the control limits defined in phase I are suitable and reliable for controlling current and future wave speed values. The isolated out-of-range points should not be interpreted as a result of a change of the wall stiffness of the monitored shaft. Any decrease of future wave speed values induced by a drop of the wall stiffness of the pressure shaft should be detected on the $\bar{x}$ chart by a permanent decrease of mean values with more or less the same global behavior of *R*. The failure of the acquisition system and/or the assessment methods should appear on the *R* chart by a high scattered pattern of points falling far outside the established control limits.

Monitoring charts for exponential attenuation coefficient

For shut-down modes of pumps and turbines, the establishment of one set of control limits for $\bar{x}$ is not possible due to the shift encountered by the φ values. The control charts can be established after collecting additional future measurements.
For the start-up modes, an $\bar{x}$ and *R* chart have been prepared. They are presented in Figs. 10(a) and 10(b). The control limits were defined by classifying the subsequent records in 45 subgroups of 4 samples each. The patterns of the plotted points in these figures do not exhibit nonrandom or a particular systematic behavior. Some points fall close or slightly outside the UCL and LCL limits. The control limits defined in this case can be used in phase II for on-line monitoring of future values of the exponential attenuation coefficient.

Conclusions

The pressure shaft of the Grimsel II pumped-storage plant has been equipped with two high sensitive pressure sensors located at its two accessible reaches at the entrance of the powerhouse (station S1) and at the butterfly valve (station S2) between the vertical surge tank and the inclined surge shaft. The water-hammer transients generated by the manoeuvres of the valves and machines during pumping and generating modes have been measured during four months between February 17 and June 10, 2011. A total number of 396 data files have been acquired continuously in time at a sample frequency of 1 kHz and they have been controlled and accessed on-line by a secured internet connection. The most relevant parts of the pressure signals were identified and analysed in detail to assess the water-hammer wave speed and to quantify the wave attenuation inside the steel-lined pressure shaft.
The special layout of the pressure shaft of the Grimsel II waterway with the inclined surge shaft situated between the upstream and downstream measurement stations and the low accuracy of the synchronization scheme between the two acquisition systems made it difficult to use the two pressure records P1 and P2 to estimate the celerity and attenuation of the water-hammer wave. Nevertheless, it was possible to monitor the shaft by processing data of the pressure records acquired at station S1. The wave speed was assessed from the FFT density spectrums while the attenuation coefficient was determined by computing the RMS of the filtered pressure signal followed by an exponential regression fitting. The monitoring charts of the mean, $\bar{x}$, and the range *R*, for the wave speed and attenuation coefficient were established based on the statistical quality control procedure.

The general patterns of points on the $\bar{x}$ and R charts reveal that the data assessment method proposed in this paper for estimating the wave speed and attenuation is stable since no change of the stiffness of the steel-lined shaft is suspected to happen in the short time duration of the monitoring campaign. Any decrease of future wave speed values and/or increase of wave attenuation coefficient induced by a drop of the wall stiffness of the pressure shaft should be detected on the monitoring charts by a permanent deviation of mean values with more or less the same global behaviour of R. The failure of the acquisition system and/or the assessment methods should appear on the R chart by a high scattered pattern of points falling far outside the established control limits. The control limits for the water-hammer wave speed can be updated after acquiring a longer series of in-situ measurements. The monitoring charts for the wave attenuation coefficient during the pump and turbine start-up modes are in control and can be used in the second phase for on-line monitoring. For the pump and turbine shut-down modes, the values of the mean attenuation coefficients have encountered a shift of about 55%.

In an ongoing research, additional measurements will be acquired to understand the global pattern behavior and to consolidate and revise the control limits of the monitoring charts of the pressure shaft of the Grimsel II power plant. Other data analysis methods such as the system identification approach will be used to characterize the physical system by estimating the frequency response, the cross-correlation and the coherence functions of the steel-lined shaft from pressure records. The results obtained by the latter approach will be compared to those which have been presented in this paper.

Acknowledgments

The study presented herein is part of the research project HydroNet (modern methodologies for the design, manufacture and operation of pumped-storage plants) funded by the Swiss Competence Center Energy and Mobility (CCEM-CH), Swisselectric research and the Swiss Office for Energy. The authors wish to acknowledge the technical support of Kraftwerke Oberhasli AG (KWO).

Notation

The following symbols are used in this paper:

c	=	complex water-hammer wave speed;
c_0	=	water-hammer wave speed;
C_r	=	radial damping coefficient per unit area of the Kelvin model;
e	=	steel liner wall thickness;
E_c	=	elasticity modulus of backfill concrete;
E_{crm}	=	elasticity modulus of the near-field rock mass;
E_{rm}	=	elasticity modulus of the far-field rock mass;
E_s	=	elasticity modulus of steel liner;
f	=	frequency;
k	=	ratio of the wave speed (c_0) to the complex wave speed (c);
K_r	=	coefficient defined in Eq. (1);
Ks_r	=	radial spring stiffness coefficient per unit area of the Kelvin model;
K_w	=	bulk modulus of water;
L	=	distance measured along the shaft axis;
M_r	=	radial additional mass per unit area of the Kelvin model;
p_i	=	internal water pressure;

r_a	=	internal radius of the near-field rock zone;
r_c	=	internal radius of backfill concrete;
r_f	=	internal radius of the far-field rock zone;
r_i	=	internal radius of the pipe or the steel liner;
t	=	time;
x	=	statistical population;
y	=	longitudinal coordinates along the shaft axis;
λ	=	wave length;
ν_c	=	Poisson's ratio for backfill concrete;
ν_r	=	Poisson's ratio for rock;
ν_s	=	Poisson's ratio for steel;
ρ_s	=	unit mass of steel;
ρ_w	=	unit mass of water;
φ	=	logarithmic decrement of the wave;
ω	=	angular frequency;

References

Beck, S. B. M., Curren, M. D., Sims, N. D., and Stanway, R. (2005). "Pipeline network features and leak detection by cross-correlation analysis of reflected waves." *Journal of Hydraulic Engineering*, 131(8), 715–723.

Burr, I. (1967). The effect of nonnormality on constants for $\bar{x}$ and R charts. *Industrial Quality Control*, 23(11), 563-569.

Coleman, H. and Steele, W. (1999). *Experimentation and uncertainty analysis for engineers*. Wiley-Interscience, New York, second edition.

Covas, D., Ramos, H., and Betâmio de Almeida, A. (2005). "Standing wave difference method for leak detection in pipeline systems." *Journal of Hydraulic Engineering*, 131(12), 1106–1116.

Ferrante, M., and Brunone, B. (2003). "Pipe system diagnosis and leak detection by unsteady-state tests. 2. Wavelet analysis." *Advances in Water Resources*, 26, 107–116.

Hachem, F.E., Schleiss, A.J. (2009). "The design of steel-lined pressure tunnels and shafts". *The International Journal on Hydropower & Dams,* 16(3), 142-151.

Hachem, F.E., and Schleiss, A.J. (2011a). "A review of wave celerity in frictionless and axisymmetrical steel-lined pressure tunnels." *Journal of Fluids and Structures*, 27, 311-328.

Hachem, F., Schleiss, A. (2011b). Detection of local wall stiffness drop in steel-lined pressure tunnels and shafts of hydroelectric power plants using steep pressure wave excitation and wavelet decomposition. *Journal of Hydraulic Engineering*, DOI: 10.1061/(ASCE)HY.1943-7900.0000478.

Hachem, F., Schleiss, A. (2011c). The influence of drop in pipe wall stiffness on water-hammer speed and attenuation. Accepted for publication in *Journal of Hydraulic Research*.

Hunaidi, O. (2006). “New Acoustic Technology for Non-Destructive Assessment of Pipe Wall Thickness”. *Workshop on Performance and Cost Targets for Water Pipeline Inspection Technologies*, Atlanta, GA.

Mallat, S.G. (1990). *A Wavelet Tour of Signal Processing*. Academic Press, San Diego, CA.

Montgomery, D.C. (2005). *Introduction to statistical quality control*. John Wiley and Sons, Inc., USA, fifth edition.

Pahl, A., Heusermann, S., Bräuer, V., and Glöggler, W. (1989). Grimsel test site - Rock stress investigations. Technical report (unpublished).

Wylie, E.B., Suo, L., and Streeter, V.L. (1993). *Fluid Transients in Systems*, facsimile edition. Prentice Hall, Englewood Cliffs, NJ.

Yourstone, S. and Zimmer, W. (1992). Non-normality and the design of control charts for averages. *Decision Sciences*, 23(5), 1099–1113.

Table of coordinates at axis (m)

Point	X	Y	Z
1	0.00	0.00	1763.50
2	578.72	0.00	2211.27
3	689.78	-30.50	2214.87
4	766.28	-42.40	2216.38
5	644.90	-51.45	2214.75
6	709.70	0.00	2336.00
7	779.43	-26.17	2336.00
8	129.83	0.00	1766.93
P1	103.83	0.00	1763.50
P2	639.93	-11.86	2214.70
a	9.89	0.00	1763.50
b	27.00	0.00	1763.50
c	36.89	0.00	1763.50
d	54.00	0.00	1763.50
e	63.89	0.00	1763.50
f	81.00	0.00	1763.50
g	90.89	0.00	1763.50

Table of reaches lengths (m)

Reach	L
1-a, b-c, d-e, f-g	9.89
a-b, c-d, e-f	17.11
g-P1	12.94
P1-8	26.46
8-2	632.05
1-2	762.34
2-P2	64.00
P2-3	49.53
3-4	98.72
3-5	49.53

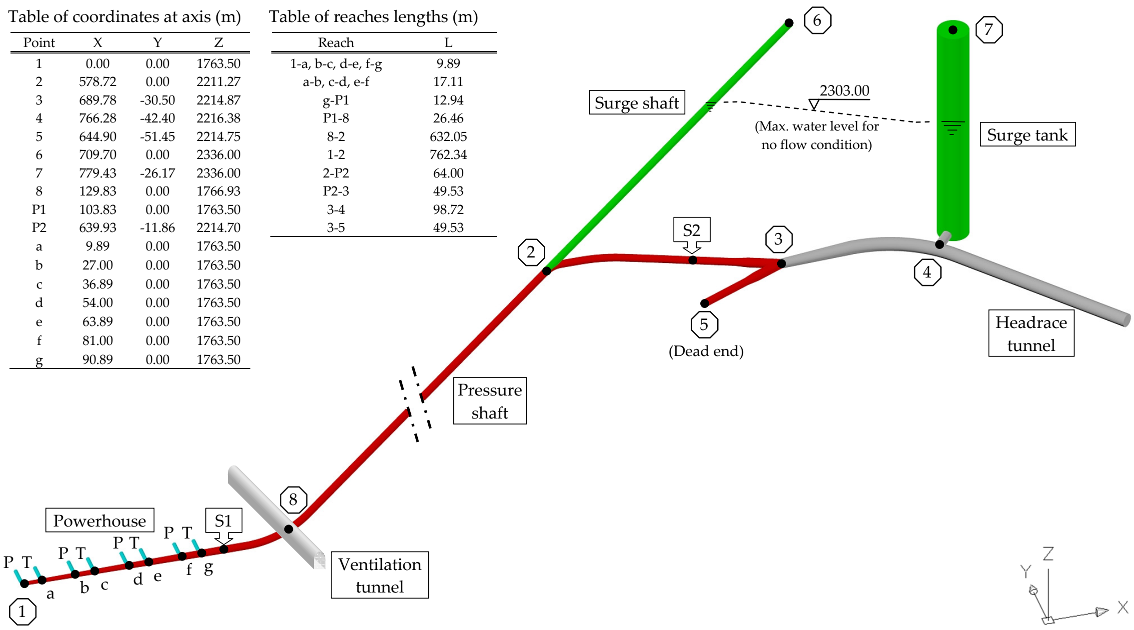

Figure 1: 3D schematic view of the high pressure side of the waterway of Grimsel II plant from the bifurcation inside the powerhouse to the downstream end of the headrace tunnel. The cross-section of the steel-lined shaft is also shown and the coordinates and lengths of the main reaches are given in the Tables.

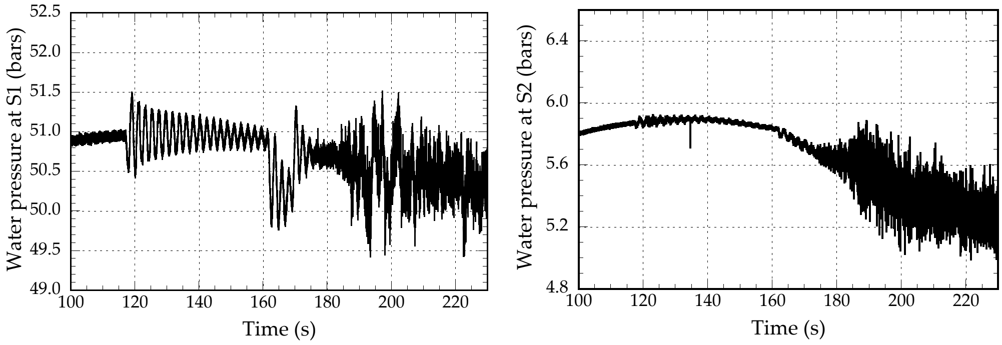

(a) (b)

Figure 2: Parts of the in-situ output pressure records used for monitoring of the pressure shaft of the Grimsel II power plant during **start-up of pumps**, (a) P1 and (b) P2 records.

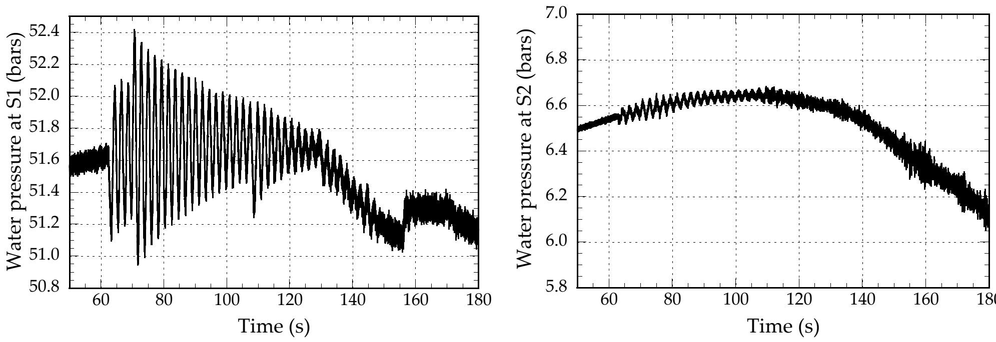

(a) (b)

Figure 3: Parts of the in-situ output pressure records used for monitoring of the pressure shaft of the Grimsel II power plant during **start-up of turbines**, (a) P1 and (b) P2 records.

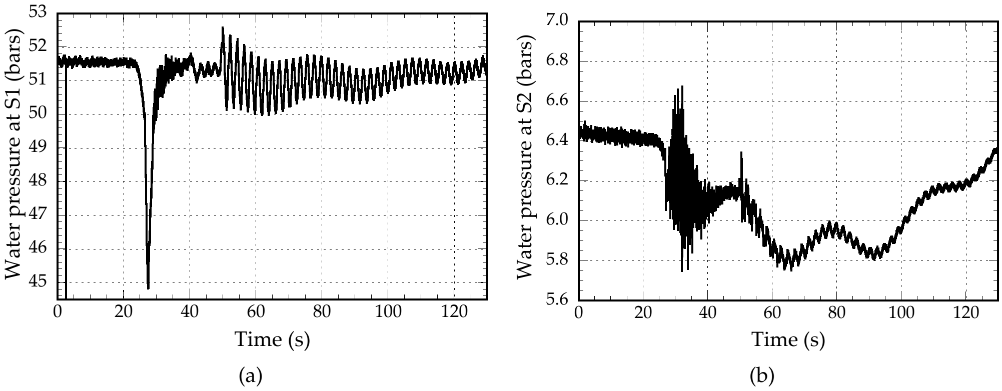

Figure 4: Parts of the in-situ output pressure records used for monitoring of the pressure shaft of the Grimsel II power plant during **shut-down of pumps**, (a) P1 and (b) P2 records.

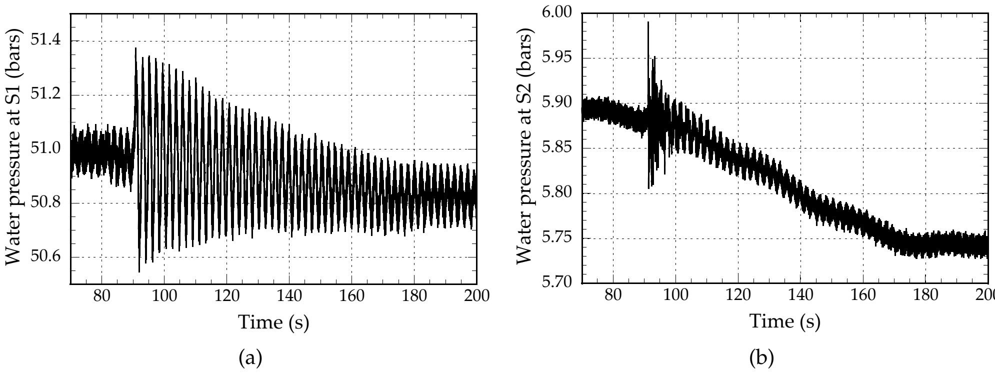

Figure 5: Parts of the in-situ output pressure records used for monitoring of the pressure shaft of the Grimsel II power plant during **shut-down of turbines**, (a) P1 and (b) P2 records.

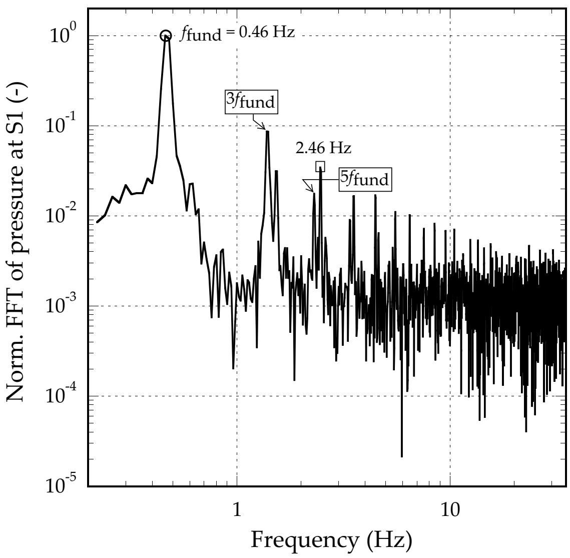

Figure 6: Normalized Fast Fourier Transform of pressure records P1 shown in Fig. 3(a).

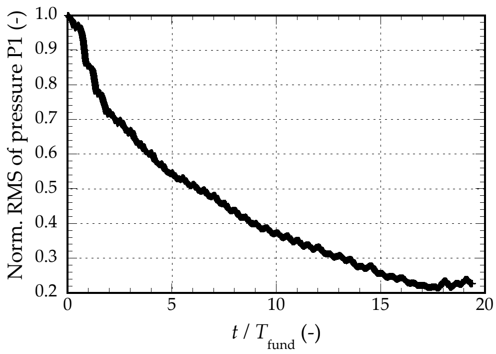

$$\mathrm{Norm(P1)} = 0.9189\,\mathrm{e}^{(-0.0860\,s)};\ R^2 = 0.993$$

Figure 7: Normalized RMS data and the exponential regression equations with their R-squared for the pressure records P1 given in Fig. 3(a).

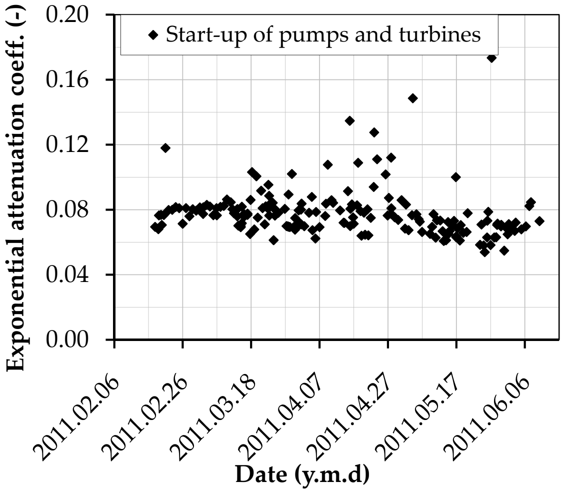

(a)

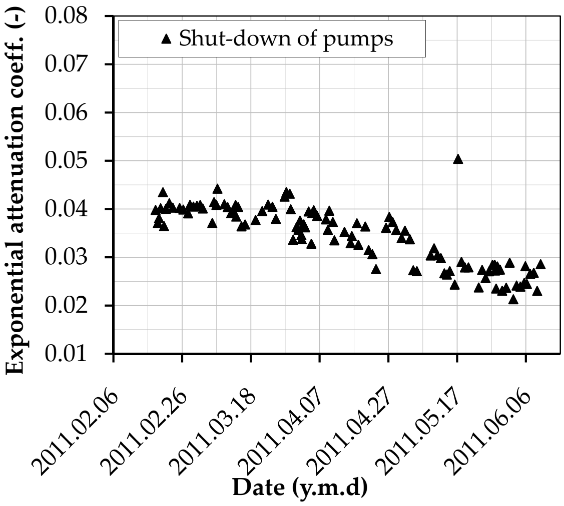

(b)

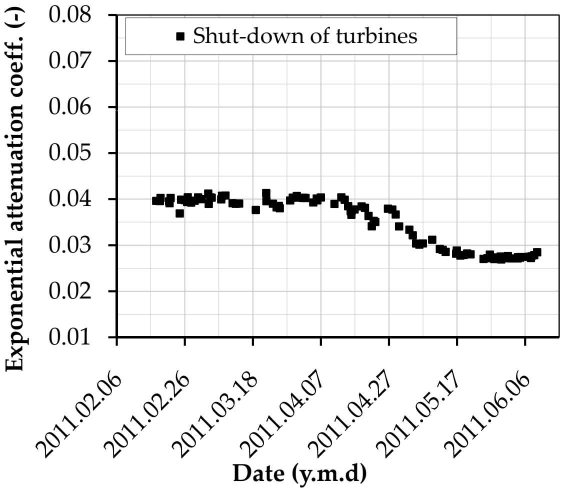

(c)

Figure 8: Dissipation coefficients values obtained from the processing of the pressure P1 records inside the shaft of the Grimsel II power plant, (a) during **start-up of pumps and turbines**, (b) during **shut-down of pumps**, (c) during **shut-down of turbines**.

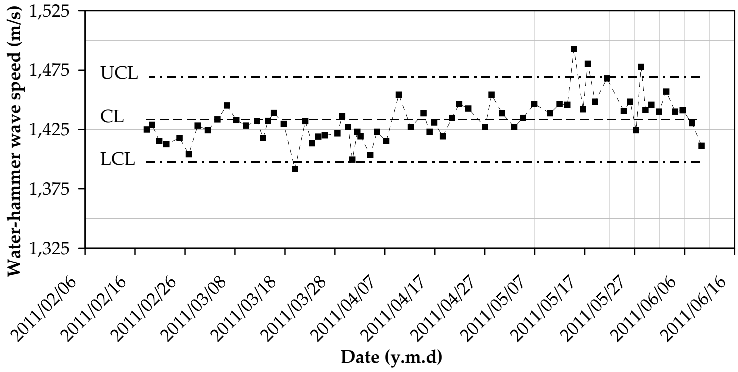

(a)

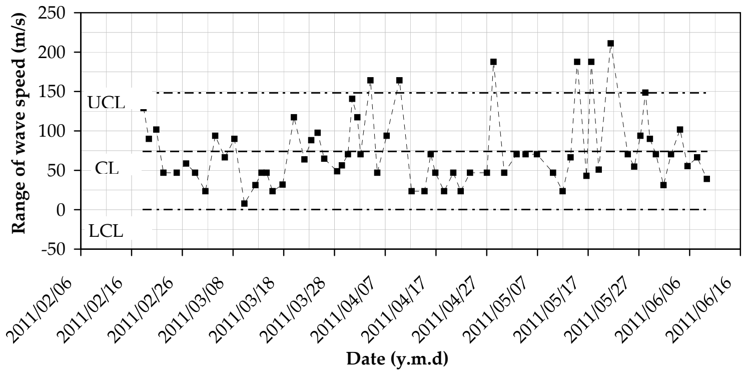

(b)

Figure 9: The monitoring charts for the water-hammer wave speed of the pressure shaft of the Grimsel II pumped-storage power plant, (a) the control of the process average or mean quality $\overline{x}$ and (b) the control of the process variability or range R chart.

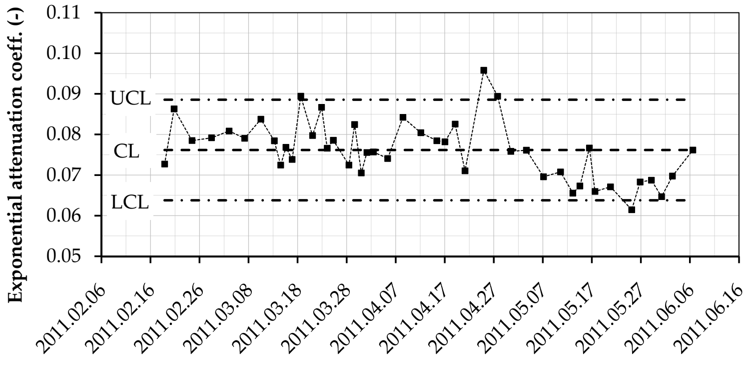

(a)

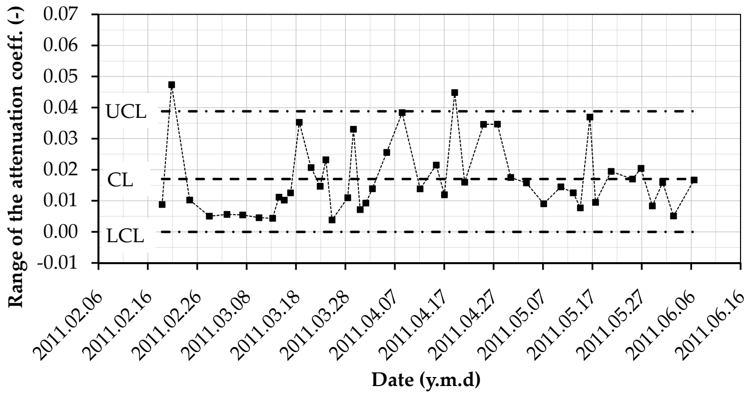

(b)

Figure 10: The monitoring charts for the exponential dissipation coefficient of the pressure shaft of the Grimsel II pumped-storage power plant during **start-up modes**, (a) the control of the process average or mean quality $\overline{x}$ and (b) the control of the process variability or range R chart.